Check for updates

Received: 10 March 2022 | Revised: 28 June 2022 | Accepted: 21 August 2022

DOI: 10.1002/rob.22117

RESEARCH ARTICLE

WILEY

A multirobot system for autonomous deployment and recovery of a blade crawler for operations and maintenance of offshore wind turbine blades

Zhengyi Jiang[1] | Ferdian Jovan[2] | Peiman Moradi[3] | Tom Richardson[3] | Sara Bernardini[4] | Simon Watson[1] | Andrew Weightman[5] | Duncan Hine[3]

[1]Department of Electrical and Electronic Engineering, The University of Manchester, Manchester, UK

[2]Department of Computer Science, University of Bristol, Bristol, UK

[3]Department of Aerospace Engineering, University of Bristol, Bristol, UK

[4]Department of Computer Science, Royal Holloway University of London, Egham, UK

[5]Department of Mechanical, Aerospace and Civil Engineering, The University of Manchester, Manchester, UK

Correspondence

Zhengyi Jiang, Department of Electrical and Electronic Engineering, The University of Manchester, Manchester, M1 3BU, UK.
Email: zhengyi.jiang-2@manchester.ac.uk

Funding information

Innovate UK, Grant/Award Number: 104821; Engineering and Physical Sciences Research Council, Grant/Award Number: EP/R026084/1

Abstract

Offshore wind farms will play a vital role in the global ambition of net zero energy generation. Future offshore wind farms will be larger and further from the coast, meaning that traditional human-based operations and maintenance approaches will become infeasible due to safety, cost, and skills shortages. The use of remotely operated or autonomous robotic assistants to undertake these activities provides an attractive alternative solution. This paper presents an autonomous multirobot system which is able to transport, deploy and retrieve a wind turbine blade inspection robot using an unmanned aerial vehicle (UAV). The proposed solution is a fully autonomous system including a robot deployment interface for deployment, a mechatronic link-hook module (LHM) for retrieval, both installed on the underside of a UAV, a mechatronic on-load attaching module installed on the robotic payload and an intelligent global mission planner. The LHM is integrated with a 2-DOF hinge that can operate either passively or actively to reduce the swing motion of a slung load by approximately 30%. The mechatronic modules can be coupled and decoupled by special maneuvers of the UAV, and the intelligent global mission planner coordinates the operations of the UAV and the mechatronic modules for synchronous and seamless actions. For navigation in the vicinity of wind turbine blades, a visual-based localization merged with the location knowledge from Global Navigation Satellite System has been developed. A proof-of-concept system was field tested on a full-size decommissioned wind-turbine blade. The results show that the experimental system is able to deploy and retrieve a robotic payload onto and from a wind turbine blade safely and robustly without the need for human intervention. The vicinity localization and navigation system have shown an accuracy of 0.65 and 0.44 m in the horizontal and vertical directions, respectively. Furthermore, this study shows the feasibility of systems toward autonomous inspection and maintenance of offshore windfarms.

Zhengyi Jiang, Ferdian Jovan and Peiman Moradi contributed equally to this study.

This is an open access article under the terms of the Creative Commons Attribution License, which permits use, distribution and reproduction in any medium, provided the original work is properly cited.
© 2022 The Authors. *Journal of Field Robotics* published by Wiley Periodicals LLC.

KEYWORDS
field robotics, multirobot cooperation, systems design, UAVs

1 | INTRODUCTION

As a consequence of increasing climate change awareness and oil shortage, research and policies for renewable energy have been gaining greater attention in recent years. The EU Green Deal, as one of the policies, aims to make the EU become the first climate-neutral continent by 2050 (Tsiropoulos et al., 2020). With this increasing demand, wind energy has become one of the most promising ways to produce renewable energy. The use of turbines has reached a global cumulative wind power capacity of 743 GW and has rapidly been increasing with 50 and 93 GW of new installations in 2019 and 2020, respectively (IRENA, 2019; Lee & Zhao, 2021). Offshore wind farms are particularly attractive as the farms and turbines could exploit stronger uninterrupted winds, be made larger, and minimize conflict of interests with other aspects of society (e.g., visual disturbance) (Bergström et al., 2014). According to IRENA (2019), offshore wind farm installations are predicted to reach 228 GW in 2030, compared to the 23 GW installed in 2018. However, due to their remote location, wind farms are exposed to unpredictable and harsh weather, which results in highly variable operational conditions and, in turn, to intense and costly maintenance operations (Zion Market Research, 2019). The current practice utilizes vessels to transport technicians and equipment to the turbines to perform close-up visual and nondestructive testing (NDT) inspections. Following this, rope access technicians are deployed to carry out maintenance wherever required. To maintain offshore wind farms performing at their optimal level using this conventional method, it costs approximately 25% of the wind turbine installation cost over 25 years of service (Nilsson & Bertling, 2007). As a comparison, the Levelized costs of electricity (LCOE) for an onshore windfarm constitutes only 5% of its total investment cost (Ren et al., 2021). This costly process can be attributed to two factors: (i) the length of turbine downtime when rope-access technicians perform close-up visual or NDT inspections, and (ii) the daily use of crew transfer vessels, including the rope access technicians for round trips to and from the farms (Kabbabe Poleo et al., 2021). Additionally, technicians are subject to health-and-safety risks due to harsh environments and weather conditions.

Recent advancement in the development of robotic platforms has opened up new opportunities in the automation of the operation and maintenance (O&M) of offshore wind farms. Employing autonomous systems to maintain offshore assets provides the benefits of reducing the cost significantly while also removing the health-and-safety risks associated with the technicians (Stetco et al., 2019). One prominent research direction in wind farm O&M is the use of blade inspection, maintenance, and repair (IMR) robots such as BladeBug (see Figure 2) where these robots are remotely operated and controlled to perform inspection and repair on wind turbine blades. However, to ensure robustness and safety of operations on and around wind turbines, many current practical implementations rely on manual processes where the deployment and retrieval processes of the IMR robots on the turbine blades are performed by rope access technicians. As such, crew transfer vessels are still required and health-and-safety risks are still present to technicians.

Within the multiplatform inspection, maintenance and repair in extreme environments (MIMREE) (Bernardini et al., 2020) project, a multirobot system is proposed to automate the process of deploying and retrieving the blade IMR robot on O&M of offshore wind farms. It is believed that multiple autonomous robots are more robust to failures and can achieve better overall performance in their execution due to their collaborative nature (Piacentini et al., 2019; Welburn et al., 2019). However, utilizing multiple heterogeneous robots, as suggested in Bernardini et al. (2020), requires robust coordination and implementation as each robot may have its set of own functionalities and roles. As shown in Figure 1, the autonomous process consists of six steps: (A) an unmanned aerial vehicle (UAV) and an IMR robot are transported by an ASV from the onshore control center to the offshore wind farms; (B) the UAV takes off with the IMR robot; (C) the IMR robot is safely deployed on the wind turbine blade by the UAV; (D) the robot is recovered by the UAV after completing its mission; (E) the UAV carries the robot and returns to the ASV; and (F) the ASV transports the entire system back to the onshore control center. The scope of this paper focuses on steps C and D, introducing a novel deployment and retrieval system to overcome the challenges in autonomously and safely deploying and recovering an IMR robot from a wind turbine blade, to fully eliminate the need for human involvement in close-up inspection and repair of offshore wind turbine blades using rope access techniques.

The main contribution of this paper is (1) novel designs of mechatronic systems for deployment and retrieval of a blade IMR robot such as a BladeBug MK II robot (see Figure 2); (2) an UAV equipped with a LiDAR-based navigation and control system; (3) a centralized AI planning software for autonomous coordination and control between the UAV and the mechatronics. These prototype systems have been developed and tested in field trials demonstrating the robustness of our proposed approach. Results show that the proposed approach is effective in retrieving an IMR robot from a wind turbine blade safely and robustly without the need for human intervention.

2 | RELATED WORK

This section lays out important developments in recent years related to our work. They are grouped into three different sections according to our most critical contributions.

2.1 | Air-based ground object retrieval systems

In recent times, helicopter hoist systems are frequently used in disaster rescue operations to perform vertical lift of a ground payload

15564967, 2023, 1, Downloaded from https://onlinelibrary.wiley.com/doi/10.1002/rob.22117 by University Di Roma La Sapienza, Wiley Online Library on [08/04/2024]. See the Terms and Conditions (https://onlinelibrary.wiley.com/terms-and-conditions) on Wiley Online Library for rules of use; OA articles are governed by the applicable Creative Commons License

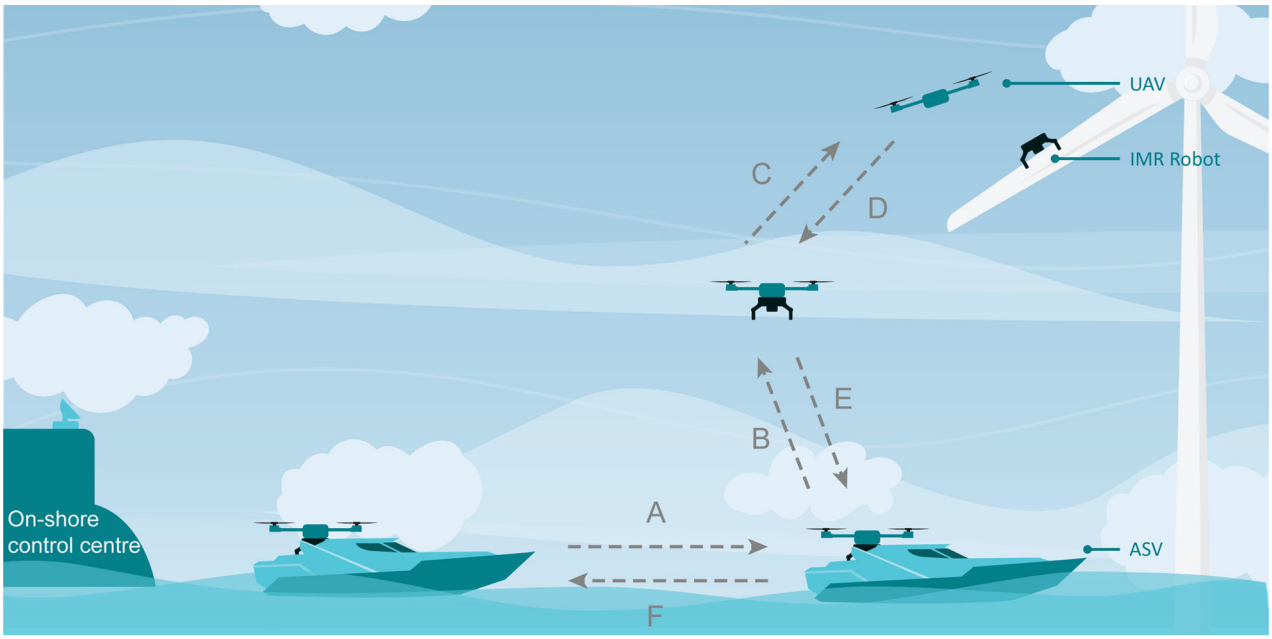

FIGURE 1 Illustration of the MIMREE multirobot system for offshore wind farm operations and maintenance

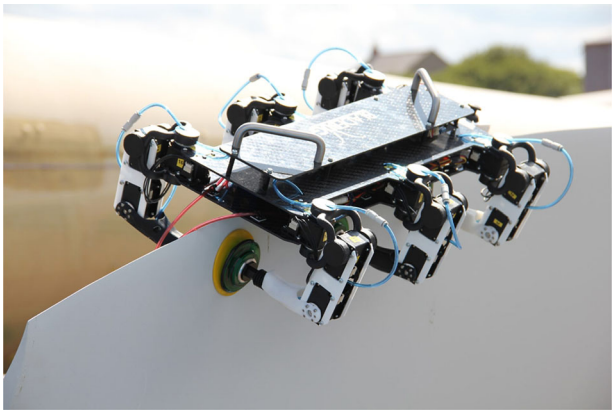

FIGURE 2 BladeBug MKII IMR robot

(Nonnenmacher & Jones, 2016). As the helicopter hovers above the payload, a rescue basket is lowered to the ground level to accommodate the payload, which is then retrieved. Such a process is often manual. The rescue basket is usually a passive device that cannot control its touchdown location or possess any equipment to grasp the payload automatically. Young (2007) described an advanced rescue basket that has two Tilt Nacelle Ducted-Fan thrusters installed on the sides, effectively transforming it into an aerial vehicle. The rescue basket can be remotely controlled to fly in the desired trajectory to reach locations inaccessible with the traditional helicopter hoist system. The technology provides local control of the slung load position which can be potentially used to drive a winch hook to engage pickup features on an IMR robot. However, miniaturization of such thrusters on a UAV of much less weight and power than a helicopter may be a challenging task. Adding autonomy to the vectored hoist may also significantly increase control complexity in a gusty environment.

Before helicopter hoist systems were developed, the Fulton surface-to-air recovery system (Heinrich et al., 2018) was used by the US military to recover ground targets. The system requires deployment of a helium balloon from the ground that sends a lift line into the sky with one end of the lift line attached to the payload. The lift line can then be captured by a V-shaped fork installed on the nose of an aircraft (Leary, 2008). However, this system is entirely manual, and there are many challenges to adopting this concept in a much smaller system using autonomous agents. First, a balloon releasing mechanism is needed on the IMR robot, which could add significant weight and increase the physical size of the robot. Second, gust wind and turbulence could cause the balloon to move violently and unpredictably, requiring an agile maneuver of the aircraft to catch the lift line, which is difficult in such an environment. Third, the lift line may be entangled in the aircraft risking failing the entire system.

Ivanovic et al. (2018) demonstrated a novel technology for retrieving a surfaced autonomous underwater vehicle (AUV) using a UAV. During a mission, a compliant net is winched down from the UAV until afloat. Once the AUV navigates itself into the net, the net is lifted, automatically contracting around the AUV. This device is specifically designed for robots with streamlined shapes that allow them to safely navigate into the net without getting entangled. However, in our case, the shape of an IMR robot is much more complex. Additionally, maintaining the net on the curved surface of a wind turbine blade is challenging, especially in a gusty environment.

Roderick et al. (2021) studied the anatomy of bird feet and developed a biomimetic UAV that uses bird-like robotic legs called stereotyped nature-inspired aerial grasper (SNAG) for its landing gear. SNAG features claws that can grasp and release objects of

15564967, 2023, 1, Downloaded from https://onlinelibrary.wiley.com/doi/10.1002/rob.22117 by University Di Roma La Sapienza, Wiley Online Library on [08/04/2024]. See the Terms and Conditions (https://onlinelibrary.wiley.com/terms-and-conditions) on Wiley Online Library for rules of use; OA articles are governed by the applicable Creative Commons License

various shapes up to 105 g in the demonstration. Thomas et al. (2013) developed an agile micro-UAV system with a gripper that can grasp an object at a high approaching velocity. The demonstrated system weighing 658 g could grasp a 27 g cylindrical target at speeds up to 3 m/s. Appius (2022) developed and tested a quadcopter with a custom Fin Ray gripper that can grasp and transport small objects of different geometries and surfaces reliably at a speed of 1 m/s. They used a motion tracking system to localize the test objects and the UAV. Inspired by eagle's talon, Tscholl et al. (2022) developed a UAV-mounted gripper system that uses hydraulically amplified self-healing electrostatic (HASEL) actuation. The above authors assumed a static lab environment and real-world environmental factors such as wind and associated gusts were not considered. In addition, the dynamics of the UAVs and the grippers were demonstrated with small and light-weight payloads that weighed, for example, less than 4% of the entire system in Thomas and Polin's system. In contrast, an IMR robot may weigh over 35% of the deployment and retrieval system.

Fiaz et al. (2018) described a passive magnetic grasping and impulsive release system for aerial transport of ferrous objects. The design used four neodymium magnets that allowed a maximum payload of 2.6 kg in a static environment. Due to the sliding effect of Coriolis force (Fiaz et al., 2017), the maximum feasible payload can become much less depending on the flying environment, and the weight, shape, and center of mass of the payload. In their field experiments, the system successfully picked up ferrous disks of 350–500 g under a wind speed of 27 kph. The pickup required the UAV to descend very close to the ferrous disks.

All above airborne ground object retrieval systems present practical methodologies in their specific use cases. However, some of them (e.g., Heinrich et al., 2018; Nonnenmacher & Jones, 2016; Young, 2007) involve complex manual processes which are difficult to automate in a compact robotic platform, and others are not suitable for retrieving a blade IMR robot for the reasons already discussed above. The magnetic grasping system (Fiaz et al., 2018) and a few seemingly straightforward approaches, for example, (a) landing the UAV on the top of BladeBug or (b) landing the UAV near BladeBug and commanding BladeBug to walk into the UAV's undercarriage, are challenging to achieve and have associated risks. These risks are mainly due to the reduced maneuver precision of a UAV in a gusty environment, which may cause the UAV to crash land, and the lack of precise leg posture control in BladeBug that may cause difficulties for the robot to navigate into the UAV's undercarriage.

2.2 | Autonomous navigation around objects

Autonomous UAV flights in the vicinity of objects are very sensitive operations for which high precision is required. Around wind turbines, rough weather conditions and uncertainty in the knowledge of the exact location of a turbine blade are the main factors to consider when designing a navigation system for this environment.

Venugopalan, Taher, and Barbastathis in Venugopalan et al. (2012) developed an algorithm for the autonomous landing of a commercially available quadrotor (AR Drone) on an autonomous kayak considering the harsh marine environment. The algorithm consists of two sections: (1) landing pad detection (image processing) and (2) control for navigation. In the first section, a landing pad was designed based on distinctive patterns and colors, and detection was carried out offline in MATLAB. A traditional PID controller was used for the control part, with a Ziegler–Nicholas method and trial-and-error approach utilized to tune the gains. Navigation was achieved through a cascade architecture where the UAV's hover mode (inner-loop) was wrapped around by the developed controller (outer-loop). A success rate of 75–80% with an accuracy of better than ±20 cm was achieved.

In other relevant research (Patruno et al., 2019), Patruno et al. presented an onboard vision-based positioning system relative to a target. To mitigate the camera field of view limitations at close distances, smaller features were integrated into larger features in the target design. Kamat and Rasane (2018) conducted a survey of autonomous navigation and collision avoidance techniques developed over the past years. Luo et al. created a LiDAR-based local navigator for a ground vehicle primarily for obstacle avoidance in an unknown environment (Luo et al., 2013). Lugo and Zell demonstrated a visual-based localization on a quadrotor based on the global location of three known markers (Lugo & Zell, 2014). In Schäfer et al. (2016), a framework, utilizing a LiDAR sensor, was presented to generate a 3D map of wind turbines for automated inspection. Obstacle avoidance path planning, fusing LiDAR data with global positioning system (GPS), was outlined.

For a UAV working near wind turbines, a navigation system based on global navigation satellite system (GNSS) is susceptible to measurement errors and loss of signals. For instance, a GNSS receiver, rather than reading direct signals, might read the reflected signals from the wind turbine structure (multipath errors). Nordin et al. (2022) have proposed two solutions: (1) visual localization and navigation, and (2) use of ultra-wide band (UWB) technology and anchor points. A second method is a challenging approach in the offshore environment as fixed anchor points are required. Additionally, the current UWB systems have an accuracy of less than 5 cm if the distance from anchor points is in the range of 50 to 75 m (Nordin et al., 2022). UWB signals can reach 200 m distances at the expense of lower accuracy.

For detecting wind turbine blade failures using UAVs, Rao et al. (2019) have utilized a Beidou satellite navigation method alongside an autonomous visual navigation algorithm. The steps used in the visual navigation system are: (1) capture images followed by (2) image preprocessing, (3) turbine tower detection and recognition, (4) turbine blade detection and recognition, and (5) turbine hub detection and recognition. One of the challenges encountered in Rao et al. (2019) is that different algorithms are required for wind turbines in different regions as the characteristics (e.g., the number of straight edges of the blades) may differ. Additionally, based on different meteorological conditions (e.g., sunny or cloudy days), the distinguishing characteristics of the background and the blades differ.

As deduced from the literature, rather than relying solely on GPS/GNSS for accurate navigation, researchers have adapted other methods among which onboard LiDAR and vision systems are

15564967, 2023, 1, Downloaded from https://onlinelibrary.wiley.com/doi/10.1002/rob.22117 by University Di Roma La Sapienza, Wiley Online Library on [08/04/2024]. See the Terms and Conditions (https://onlinelibrary.wiley.com/terms-and-conditions) on Wiley Online Library for rules of use; OA articles are governed by the applicable Creative Commons License

popular. In this paper, an approach merging GNSS localization with LiDAR data has been adopted.

2.3 | Cooperation and coordination amongst autonomous agents

Inspired by Bernardini et al. (2020), in this study, inspecting components of a wind turbine that might be faulty and repairing them is performed by heterogeneous robots and, in particular, UAVs and IMR robots, as it is believed that multirobot systems tend to be more robust to failures and achieve better performance in their execution. However, the approach of utilizing heterogeneous robots requires solid coordination, high-level cooperation, and the proper execution tools to achieve autonomy. Furthermore, it becomes more challenging when the autonomous system is employed in remote environments where environments are harsh and supervisory operators are not within visual line of sight (VLOS). As a result, many practical implementations prefer to rely on a single platform system with an operator within VLOS, limiting the effectiveness and benefits of full multirobot solutions (Carreno et al., 2019). For example, semiautonomous drones have achieved some maturity in the inspection operations of offshore wind farms.

Recent work has tried to integrate multirobot systems imbuing cooperation and coordination into the system in the context of extreme environments. Piacentini et al. (2019) considered multirobot problems using homogeneous UAV fleets for search-and-tracking applications. Fernandez-Gonzalez et al. (2017) utilize a centralized multirobot manager to coordinate several robots in maritime applications. They demonstrated a good result on how the planner synchronizes coordinated actions on multirobot problems. Both works utilized a well-defined planning language called PDDL Fox and Long (2003) to model missions, which is defined as planning problems, and how each system should interact and coordinate with one another in achieving the missions, which is defined as the planning domain. Both the problems and the planning domain were fed and translated by a planner to get a plan, that is, a series of actions, for each individual robot to execute. However, these works consider only homogeneous robots with similar capabilities, which limits their applicability in contexts with heterogeneous robots.

Unlike the works above, the involvement of different types of robots in this study means that each type has a different set of actions. This differentiation of actions among different robots creates coordinated actions that require more complex low-level control that not only involves the main robot but also requires the partner's robots to be actively engaged in. For example, the implementation of retrieving an IMR robot requires the robot controller to perform a series of actions such as preparing its attaching features, orientating the robot in an agreed direction, and performing an embrace position for the retrieval while, on the other side, the UAV flies toward the IMR robot and prepares its attaching module.

Due to the complexity of coordinated actions in heterogeneous robots, there are few works in this field. Carreno et al. (2019) adopted a combination of a mission-focused strategy and temporal planning to tackle multirobot systems involving underwater vehicles and autonomous surface vessels (ASV) for subsea oil rigs investigation. In his other work in Carreno et al. (2022), a similar approach was employed to tackle multirobot systems involving UAVs and Clearpath Husky robots for offshore energy platforms. Although cooperation across different types of robots in their application was very limited, Carrenno et al. demonstrated that temporal planning in combination with PDDL was capable of tackling complex actions with multiple robots, especially when agents must work concurrently and execute actions as part of joint plans. With its ability to handle concurrent actions in a multirobot system, the concept proposed in Carreno et al. (2019) is used within this study. An improvement is proposed to further validate the concept and extend the work by (1) involving different robot types such as UAVs and IMR robots from different domains and (2) injecting more complex coordinated and concurrent actions.

3 | MECHATRONIC SYSTEMS FOR DEPLOYMENT AND RETRIEVAL

Three mechatronic systems, including the robot deployment interface (RDI), the link-hook module (LHM), and the on-load attaching module (OLAM), have been developed for deployment and retrieval of an IMR robot, that is, BladeBug MK II. As briefly introduced in Section 1, BladeBug MK II is a relatively compact hexapod designed as an experimental wind turbine blade IMR platform. It is approximately 450 mm in length, 360 mm in width, and 160 mm in height with a mass of 4.5 kg. Figure 3 shows the integration of the mechatronic systems with BladeBug and a UAV platform named Goliath, forming

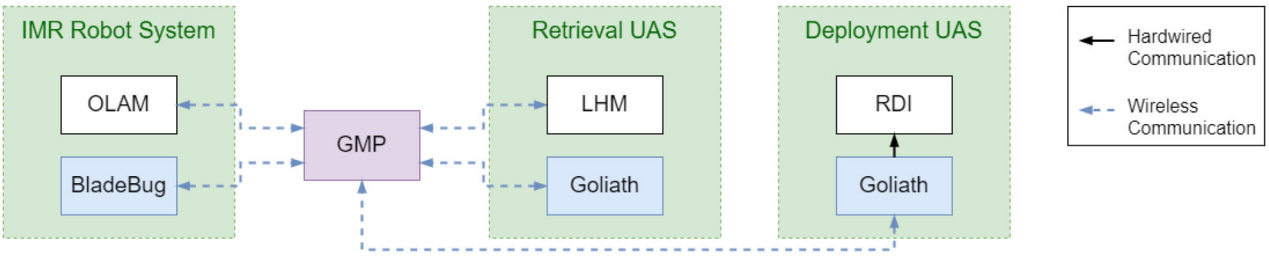

FIGURE 3 System diagram for the deployment and retrieval mechatronic systems

15564967, 2023, 1, Downloaded from https://onlinelibrary.wiley.com/doi/10.1002/rob.22117 by University Di Roma La Sapienza, Wiley Online Library on [08/04/2024]. See the Terms and Conditions (https://onlinelibrary.wiley.com/terms-and-conditions) on Wiley Online Library for rules of use; OA articles are governed by the applicable Creative Commons License

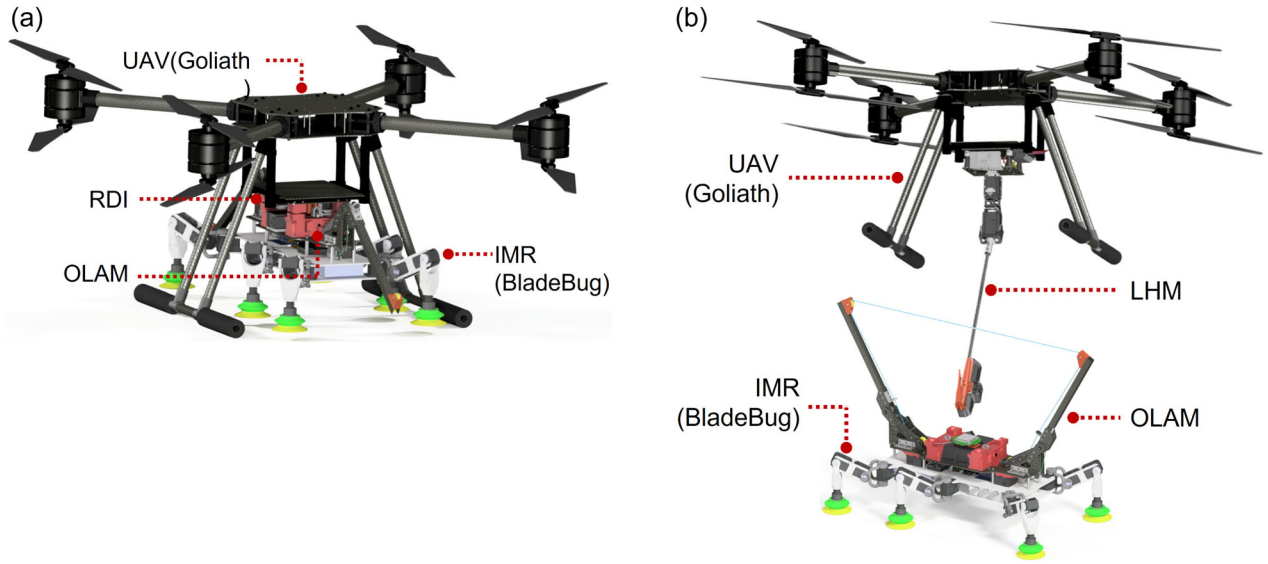

FIGURE 4 (a) The UAS for deployment (Goliath + RDI) and the IMR robot system (OLAM + BladeBug); (b) The UAS for retrieval (Goliath + LHM) and the IMR robot system

three major systems, that is, IMR robot system, retrieval UAV system (UAS), and deployment UAS. The global mission planner (GMP) is the brain that collects feedback from different robotic systems, calculates a mission plan, and broadcasts system-specific instructions for performing a coordinated operation.

CAD representations of the major systems are shown in Figure 4. As illustrated, Goliath is a large coaxial octocopter constructed from a 3DXR-IND10000 UAV frame, with a payload capacity of 6 kg[1] and a trapezoidal cube-shaped undercarriage space of 320 mm (top) × 480 mm (bottom) × 250 mm (height). Eight X-U8II-KV85 motors with MF2815 propellers and ALPHA 60A HV electronic speed control (ESC) are chosen for the UAV to provide the needed lift and resistance to wind. Specifications of Goliath are provided in Table 1. The mechatronic systems, in specific, refer to the robot deployment interface (RDI), the link-hook module (LHM), and the OLAM. RDI and LHM are part of the systems for deployment and retrieval, respectively, that are mounted in the undercarriage of Goliath. The OLAM is attached to BladeBug providing coupling interfaces for both the RDI and the LHM.

Detailed designs of the mechatronic systems are discussed further in this section, and GMP is discussed in Section 5.

3.1 | Deployment and retrieval procedures

The proposed aerial-based deployment and retrieval system emphasizes the safety of the assets, such as wind turbines, and operational reliability when flying in a gusty environment with a heavy payload (at least 4.5 kg).

[1]A quantity of 15 kg is the designed payload capacity of the UAV but restricted to 6 kg per UK Civil Aviation Authority regulations.

TABLE 1 Specifications of Goliath UAV

Parameters	Value
Dimension, overall (mm)	(L × W × H) 800 × 800 × 500
Mass (kg)	14
Payload capacity (kg)	6
Flight computer	Black Pixhawk Cube
Firmware	ArduCopter (4.0.2)
Communication	868 Mhz RFD
GPS	Ublox, F9P

Figures 5 and 6 illustrate the deployment and retrieval procedures used by the proposed system, respectively. As can be depicted, the deployment procedures involve four stages and assume the system is prepared onshore where the IMR robot system is manually coupled with the UAS and locked in the undercarriage. As the UAV arrives at the waypoint near the target wind turbine blade, the blade surface must be scanned to determine a safe location for deployment. Details of this technology are introduced in Section 4. The IMR robot system is only released when the UAS lands securely to ensure the safety of the wind turbine and the robotic systems. After the IMR robot system is safely deployed on the blade, the UAS returns to a designated area on the ASV.

As the IMR robot system completes its mission on the wind turbine blade, it communicates with GMP to request recovery. The retrieval UAS first navigates near the wind turbine blade based on GPS coordinates, and meanwhile, the OLAM unfolds itself and prepares for engagement. After the GMP confirms the OLAM is ready for engagement, the UAS aligns with the OLAM using RTK GPS and performs an engagement maneuver. Coupling between the two

15564967, 2023, 1, Downloaded from https://onlinelibrary.wiley.com/doi/10.1002/rob.22117 by University Di Roma La Sapienza, Wiley Online Library on [08/04/2024]. See the Terms and Conditions (https://onlinelibrary.wiley.com/terms-and-conditions) on Wiley Online Library for rules of use; OA articles are governed by the applicable Creative Commons License

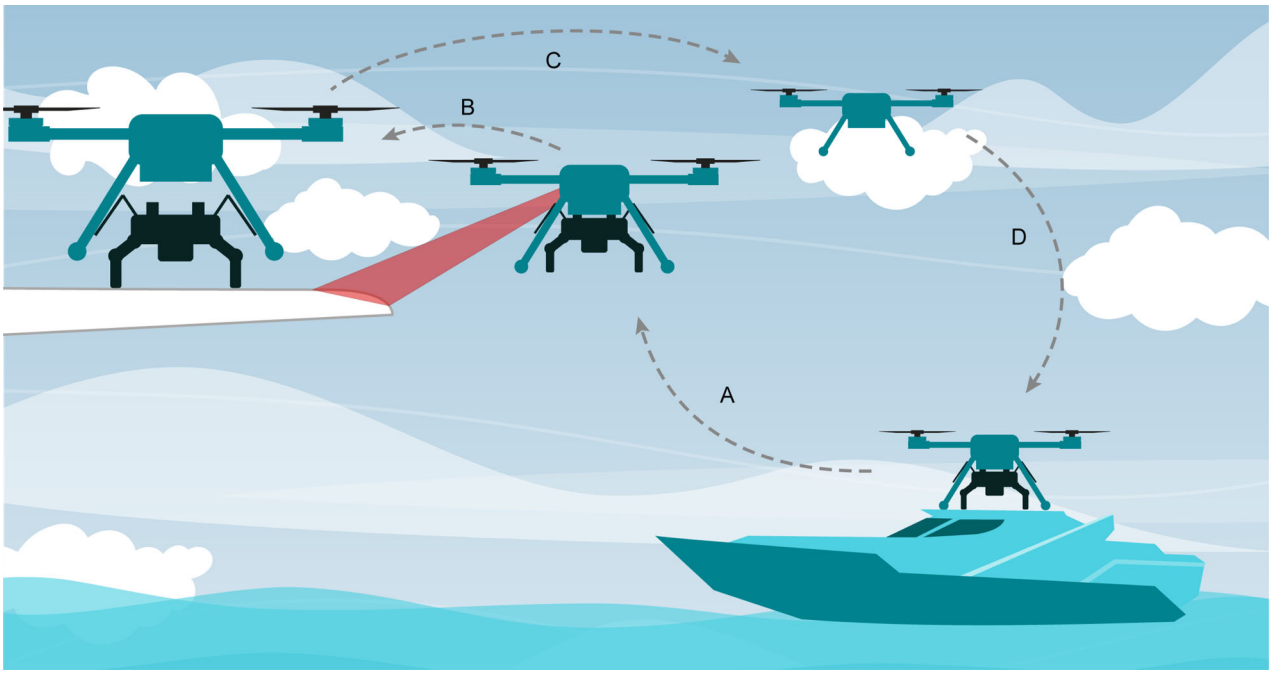

FIGURE 5 BladeBug deployment procedures: (A) the deployment UAS launches from the ASV carrying BladeBug, and scans the blade surface to locate a safe landing spot; (B) the UAS navigates to the landing spot, slowly descends to land and deploys the payload; (C) the UAS carefully takes off from the turbine blade, and; (D) returns to the ASV.

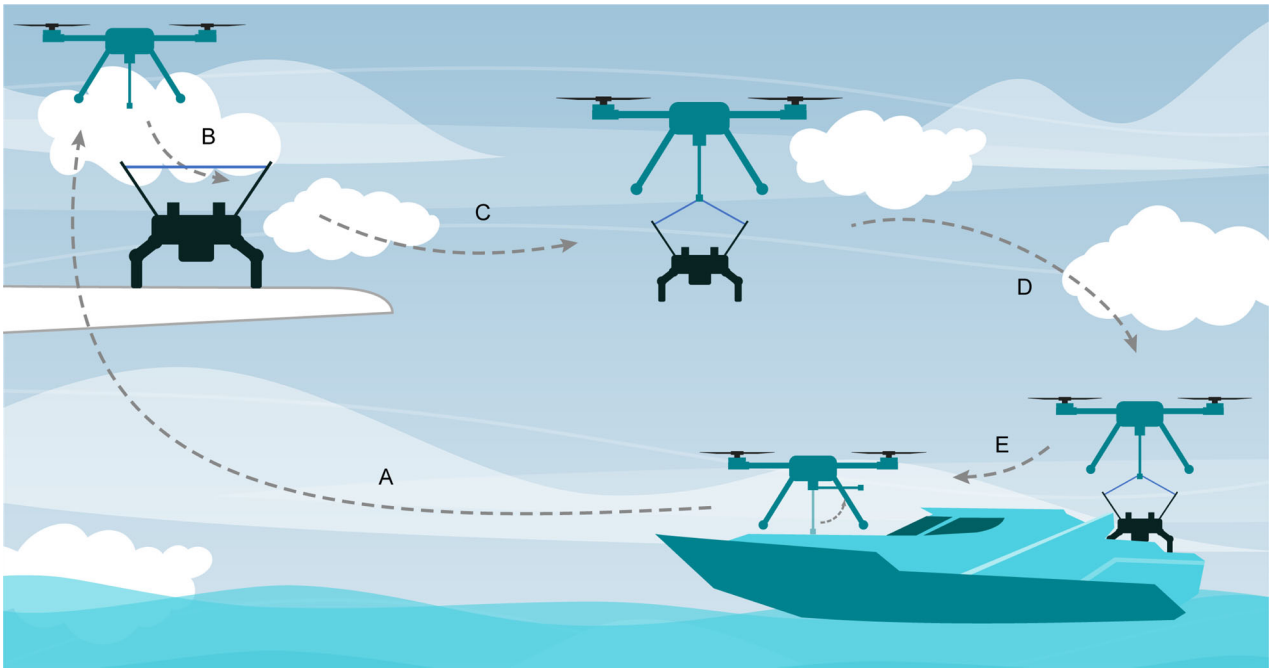

FIGURE 6 BladeBug retrieval procedures: (A) the retrieval UAS takes off from the ASV and navigates near the wind turbine blade; (B) the UAS locates and aligns with the OLAM using RTK GPS, and flies across it to engage the pickup mechanism; (C) the UAS lifts up and carries the IMR robot system to the ASV; (D) the UAS releases its payload, and; (E) the LHM folds up and the UAS proceeds to land.

15564967, 2023, 1, Downloaded from https://onlinelibrary.wiley.com/doi/10.1002/rob.22117 by University Di Roma La Sapienza, Wiley Online Library on [08/04/2024]. See the Terms and Conditions (https://onlinelibrary.wiley.com/terms-and-conditions) on Wiley Online Library for rules of use; OA articles are governed by the applicable Creative Commons License

systems is achieved by engaging and locking the hook mechanism in the LHM with the pickup line in the OLAM, details of which are described in Sections 3.4 and 3.2. The retrieval strategy is designed to avoid hovering or performing quick, agile maneuvers that are difficult for Goliath to execute safely in a windy (gusty) environment. Instead, the engagement maneuver only requires the UAV to fly in a straight trajectory for coupling with the OLAM, increasing safety and reliability in operation and reducing the risk of damaging valuable assets. After the LHM detects successful engagement, the UAS returns to the ASV and releases the IMR robot system. Finally, the LHM folds up to allow the UAV to land on the ASV safely.

3.2 | On-load attaching module

The OLAM, weighing 1.91 kg, is mounted on BladeBug as an integrated module that contains features for coupling with the UAV-mounted deployment and retrieval modules, that is, RDI and LHM. Two deployment interface blocks, as shown in Figure 7, are designed to couple with the RDI for deployment tasks. The arms are actuated by two Dynamixel XL430 servos to be folded down to avoid interfering with the safe operation of the UAV rotors. During retrieval stages, the arms of the OLAM are raised to support a pickup line straight across the top. The tension in the pickup line is automatically adjusted by a line tension control system that contains two custom tension sensors and a servo motor (Dynamixel XL430). The two arms form a trapezoid engagement window of 725 mm wide at the top and 340 mm at the bottom with a height of 325 mm. The large window is designed to accept a wide range of variations in the engaging hook position. Such variation can be attributed to several factors, including RTK GPS error (typically 20 mm), UAV path following error, and lateral swing of the hook.

The GPS coordinates and heading are derived from an RTK GPS module and a Pix32 flight computer in the controller compartment and wirelessly transmitted to GMP by a Sik 433 MHz telemetry module along with the system's status. The controller compartment also houses an OpenCM9.04 controller with an OpenCM485 expansion board for controlling all the servo motors.

3.3 | Robot deployment interface

The RDI, as part of the deployment system, is mounted on Goliath, as can be seen in Figure 4a. It can be coupled with the interface on OLAM, which is attached to BladeBug, for locking the IMR robot system in the undercarriage of Goliath and releasing the system when requested.

As shown in Figure 8, the RDI has a relatively simple construction, where two servo locking devices (Tarot TL2961-02) are used as the locking and releasing mechanism and four guide blocks are designed for accurate and repeatable alignment with the interface on the OLAM. The RDI is designed to carry a payload of maximum 10 kg and operates with PWM input from the UAV directly with a low power consumption of maximum 2.5 W.

3.4 | Link-hook module

The LHM consists of three major parts, a controller compartment, a 2-DOF hinge and a hook as shown in Figure 9. The hinge is actuated by two Dynamixel MX106 servos providing motions in the pitch and roll directions of the aircraft. The hook, connected with the hinge by a 1 m carbon fiber tube, is designed for minimum power consumption

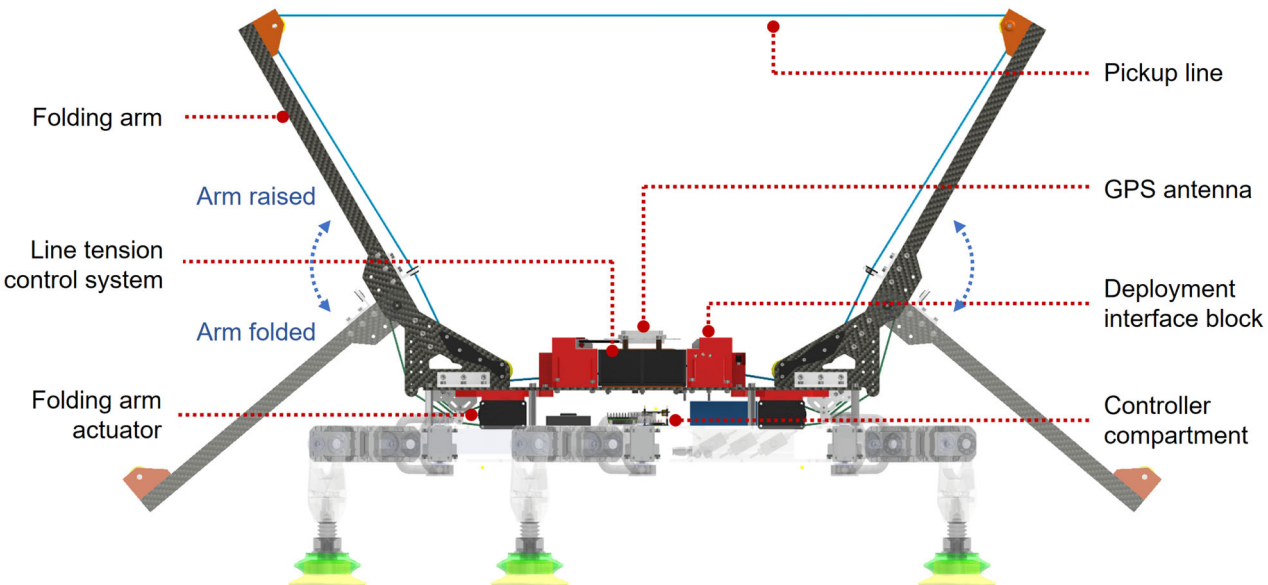

FIGURE 7 Side view of the on-load attaching module (OLAM). The folding arm can be folded down as indicated by the blue arrows.

15564967, 2023, 1, Downloaded from https://onlinelibrary.wiley.com/doi/10.1002/rob.22117 by University Di Roma La Sapienza, Wiley Online Library on [08/04/2024]. See the Terms and Conditions (https://onlinelibrary.wiley.com/terms-and-conditions) on Wiley Online Library for rules of use; OA articles are governed by the applicable Creative Commons License

to reduce the needed battery capacity. Low power consumption is achieved by having a semipassive hook opening and closing mechanism. The hook can be opened by the payload's self-weight and, by incorporating a tension spring, automatically returns to the closed position after releasing the load. The closed position can be locked by a lead screw system driven by a Dynamixel MX28 servo. A photoelectric sensor in the hook detects movement in the tension spring, which acts as a payload engagement detection mechanism. The LHM is controlled by an OpenCM9.04 controller with an OpenCM485 expansion board. A Sik 433MHz telemetry module is used to enable wireless communication with GMP.

The use of an actuated hinge between the UAV and the hook, as opposed to a solid connection or an uncontrollable connection (e.g., winch rope), serves three purposes: first, to avoid a rigid coupling between the LHM and the UAV to reduce flight control complexity; second to enable active control of the position of the link and the hook, and; third, to reduce swing motion of the hook during the lineup and engagement stage. In the current implementation, the link and the hook are only required to be controlled and positioned in the "parked" position where the link and the hook are folded up to a position that does not obstruct UAV landing, as shown in Figure 6

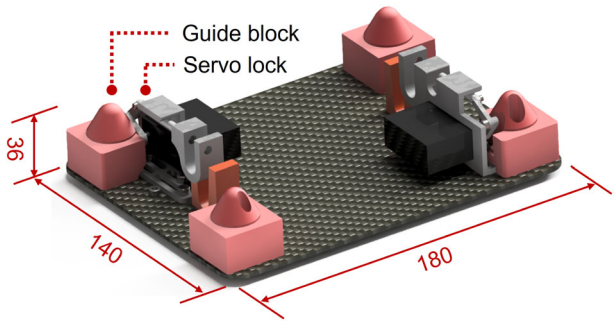

FIGURE 8 CAD design and specifications of the robot deployment interface (RDI), dimension units in mm (Mass = 0.34 kg, payload capacity = 10 kg, and rated power consumption = 2.5 W).

(Stage D). Swing motion reduction is necessary because the nonrigid setup may result in significant swing motion during the flight, which could cause the hook to miss the pickup line. Swing motion reduction can be achieved in both passive and active manners. Due to magnetic induction, rotation of the servos caused by swing motion produces an electromotive force that opposes the direction of rotation, providing passive dampening to the swing motion. In an active swing reduction mode, both servos operate in their built-in current control algorithm. By setting the current target to zero, motors are driven in the opposite direction of the swing motion, which reduces the current induced by the back EMF generated by the swing motion.

4 | UAV NAVIGATION AND CONTROL NEAR WIND TURBINE BLADE

To navigate around wind turbine blades, specifically for precisely deploying the IMR robot, a method combining GNSS and LiDAR localization is utilized. Initially, GNSS is used to take the UAV to a predetermined location in front of the target turbine blade. At this stage, a scanning LiDAR is employed to detect the blade, and a control law, a combination of position and velocity commands, is utilized to guide the UAV to the highest point on the blade's cross-section. A prototype multirotor in an *H* configuration was developed to validate the developed algorithm, Figure 10.

The components used in the prototype UAV have been summarized in Table 2 below. To scan the vertical plane, a Lightware (LW20) LiDAR has been attached to a servo which has been mounted to the front of the UAV. This system has been calibrated in a lab environment to find the relationship between the input PWM to the servo and the LiDAR angle to the horizon. Figure 11 illustrates how a LiDAR scanning is conducted, the blue region being a typical scan range, along with the reference frames of the blade cross-section and the LiDAR. The scanning angle resolution is controlled through the input PWM to the servo.

Wing detection is achieved by defining a threshold and detecting the jumps in the measured range vector, as can be seen in Figure 12.

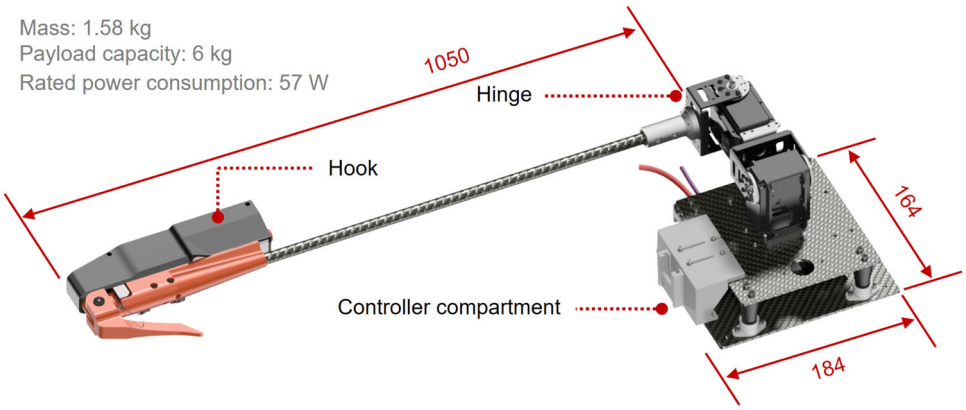

FIGURE 9 CAD design of the link-hook module, dimension units in mm

15564967, 2023, 1, Downloaded from https://onlinelibrary.wiley.com/doi/10.1002/rob.22117 by University Di Roma La Sapienza, Wiley Online Library on [08/04/2024]. See the Terms and Conditions (https://onlinelibrary.wiley.com/terms-and-conditions) on Wiley Online Library for rules of use; OA articles are governed by the applicable Creative Commons License

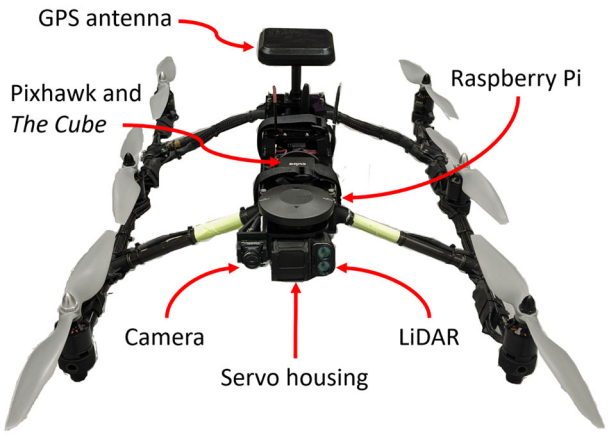

FIGURE 10 The prototype multirotor (*H* configuration)

TABLE 2 Components used in the prototype multirotor

System	Component
Flight computer	Black Pixhawk Cube (ArduCopter)
GPS	Ublox, F9P
LiDAR	Lightware LW20
Telemetry	RFD 868 modem

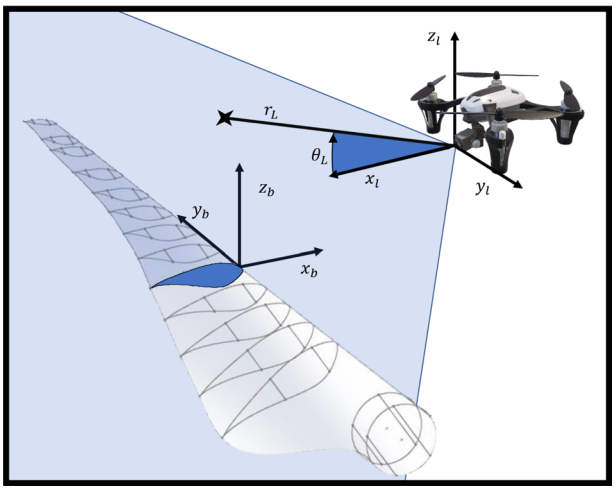

FIGURE 11 Illustration of the reference frame of the LiDAR and the reference frame of the scanned cross-section

The landing target is then defined as the highest point on the detected blade.

Figure 13 shows the navigation waypoints in landing the UAV on a turbine blade. The first two waypoints are reached by sending position commands in the local coordinate frame of the UAV. An outer loop proportional velocity controller is then developed and utilized to get to waypoints 3 and finally 4 (landing target). A block diagram of the navigation algorithm can be seen in Figure 14.

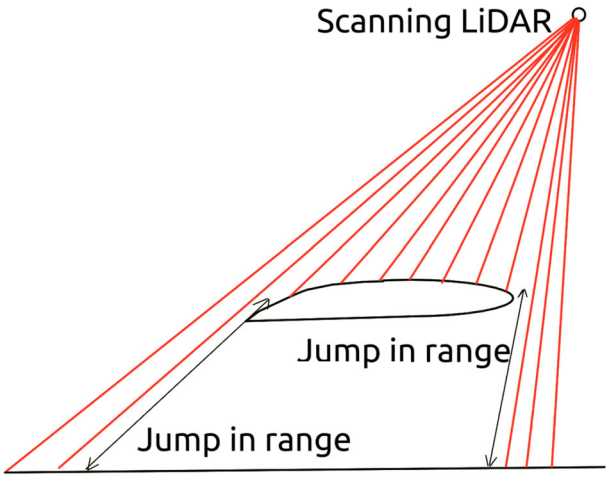

FIGURE 12 A typical LiDAR scan showing the jumps in range vector (red lines)

5 | GLOBAL MISSION PLANNING SYSTEM

To automate missions to inspect, repair, or maintain wind turbines involving heterogeneous robots, a central control manager is necessary to (1) create a coordinated plan to complete the mission and (2) monitor the execution of the plan across robots to avoid any failure. We call this central control manager *Global Mission Planner*. The global mission planner (GMP) consists of three main parts (see Figure 15): a mission planner (MP), APM Planner 2 ground control station (GCS), and MAVLink Parser (MAVROS). The GCS is used to monitor all autonomous robots and it also represents a safety layer with the capability to override the robots' autonomy when needed. MAVROS[2] is a ROS package that converts the MAVLink communication used by the UAV and the IMR robot to the ROS message system and vice versa. It provides the state of the vehicles, including battery information, odometry, and connection status. The package is also used to control the UAV and the blade IMR robot via position and velocity controllers. A similar design has been tested in O&M wind farm simulation where a GMP manages a fleet of UAVs, blade IMR robots, and autonomous surface vessels (ASV) (Jovan & Bernardini, 2021). For this study, we stripped down the control of the ASVs, as shown in Figure 15, due to the difficulty of using a real ASV for our experiments.

5.1 | Planning domain and execution process

Inspired by the work of Carreno et al. (2019), our mission planner module consists of three software packages: a planner based on a temporal PDDL solver, a problem generator, and a knowledge base. The MP module is integrated with ROS to align it with the MAVROS

[2]https://github.com/mavlink/mavros

15564967, 2023, 1, Downloaded from https://onlinelibrary.wiley.com/doi/10.1002/rob.22117 by University Di Roma La Sapienza, Wiley Online Library on [08/04/2024]. See the Terms and Conditions (https://onlinelibrary.wiley.com/terms-and-conditions) on Wiley Online Library for rules of use; OA articles are governed by the applicable Creative Commons License

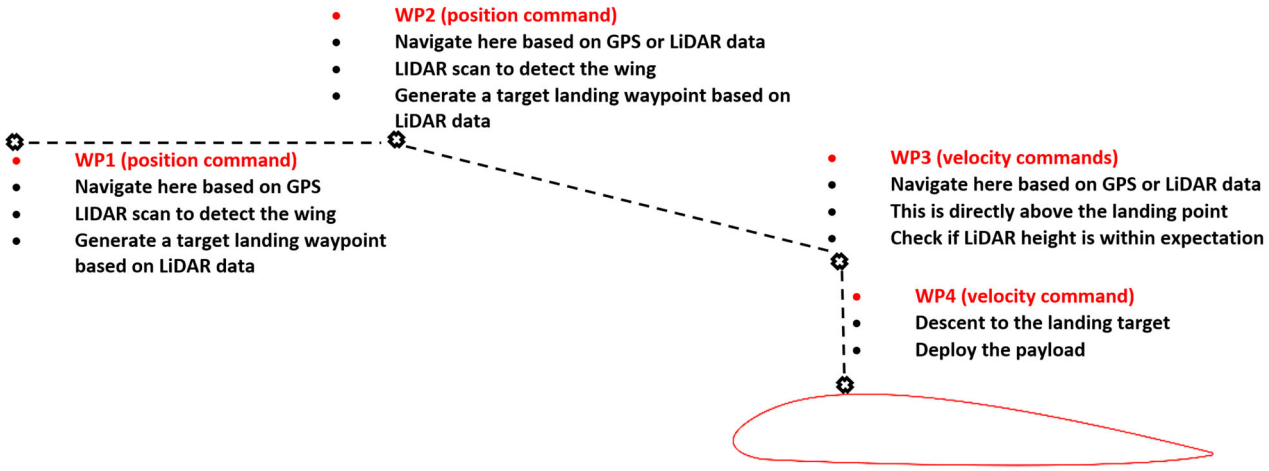

FIGURE 13 Stages of landing and deploying the IMR robot on wind turbine blade

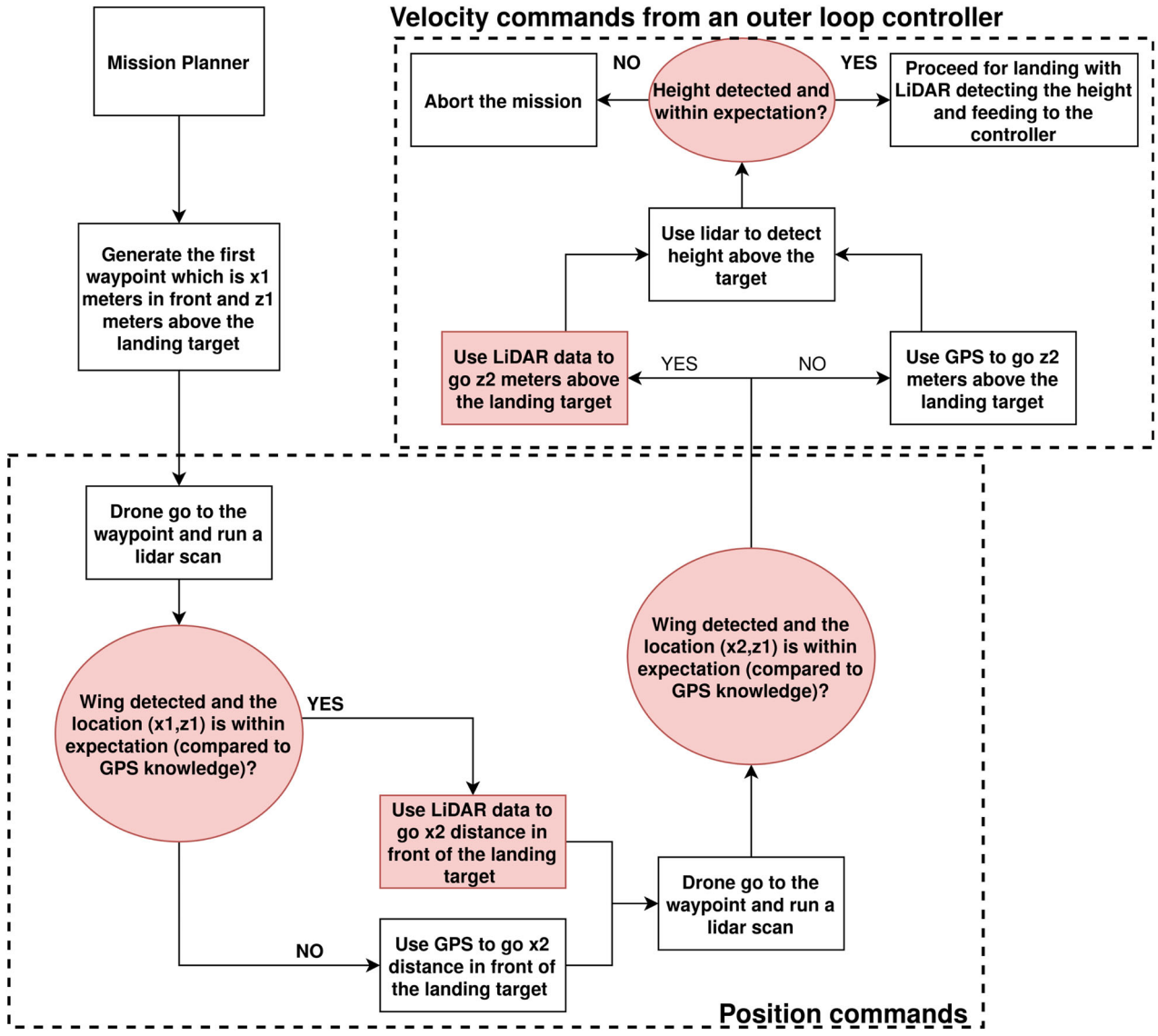

FIGURE 14 Block diagram of the navigation algorithm for landing on a wind turbine blade

15564967, 2023, 1, Downloaded from https://onlinelibrary.wiley.com/doi/10.1002/rob.22117 by University Di Roma La Sapienza, Wiley Online Library on [08/04/2024]. See the Terms and Conditions (https://onlinelibrary.wiley.com/terms-and-conditions) on Wiley Online Library for rules of use; OA articles are governed by the applicable Creative Commons License

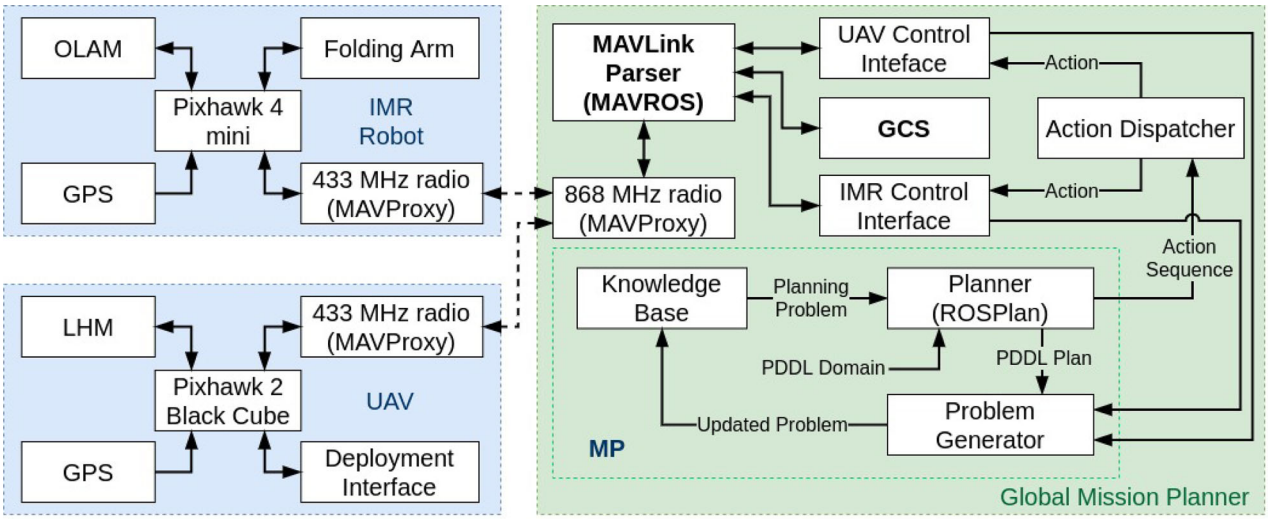

FIGURE 15 Multivehicle autonomy architecture focusing on the global mission planner module

package that relays information from and sends actions to the UAVs and the IMR robots. We utilize the ROS-based planning framework *ROSPlan* (Cashmore et al., 2015) for this purpose. ROSPlan provides all necessary components, including PDDL-solvers and interaction between a PDDL-solver and ROS. We use the temporal PDDL-solver, POPF (Coles et al., 2010), for our experiments. Temporal planning is capable of dealing with multirobot planning problems since time is modeled explicitly: individual actions for different robots can be scheduled and executed in parallel. A temporal PDDL-solver is able to generate a mission plan, that is, a series of actions, given a problem description (PDDL problem) and a domain description (PDDL domain). Our planning domain[3] describes 13 different actions spread across multiple robot types with all their constraints (e.g., battery/fuel level) and preconditions (e.g., the UAV must be airborne to pick up the blade IMR robot). We formulated our domain based on input from experts and technicians in the offshore energy field. Our domain is, however, general; it can be directly employed in the operation and maintenance (O&M) of wind turbines of various types, and it can be extended to O&M of other assets.

The problem generator translates incoming information from the UAV control interface and the IMR robot control interface into information that can be used for planning and monitoring. The information includes the robot states, robot heading, their capabilities, their battery states, sensor data, and the operating environment (e.g., wind turbines' position and their corresponding position). This information is then stored in the knowledge base (KB) module. The stored information is later used to generate missions, that is, PDDL problems.

At the earliest step, missions, such as *inspect wind turbine A with a UAV* and *inspect wind turbine A with a blade IMR robot*, are requested by a remote human operator. Information about the robots' states and sensors' availability is collected and stored in the KB module. A PDDL problem description is constructed, and a plan is generated by ROSPlan (see Table 3 for an example). The action dispatcher module disassembles the plan into individual actions according to (1) the time when the action must be executed, (2) the robot responsible for executing the action, and (3) the duration to execute the action. Each action is then distributed to its corresponding robot when the time to execute it arrives. The actions dispatched by the action dispatcher module are high-level actions describing the capabilities of each robot defined in the PDDL domain. Each robot's control interface (i.e., UAV control interface module, and IMR robot control interface) decides how the high-level actions are executed. For example, the low-level implementation of the action `uav_deploy_imr(?uav,?imr,?uav_wp,?imr_wp)` requires the use of our novel technique of UAV navigation around a wind blade, which is described in Section 4.

5.2 | Monitoring and replanning strategy

Automating the maintenance process using a multirobot system based on temporal planning has the potential of significantly reducing the costs spent annually because automation with parallel actions typically makes the process efficient. However, in practice, the efficacy of a planning-based system depends on how accurately the domain experts design the planning domain and how precisely the problem description represents the world and its operating conditions. Inaccuracies in any of those two may lead to inefficient plans and mission failures.

In our approach, the GMP tries to maintain states of the world that are as accurate as possible by reducing the discrepancy between the expected states, that is, the conditions of the world resulting from simulating action of a generated plan, and the actual states, that is, the actual conditions obtained when a robot executes an action of the generated plan. These discrepancies usually come from sensor/

[3] https://github.com/ferdianjovan/mimree_executive

15564967, 2023, 1, Downloaded from https://onlinelibrary.wiley.com/doi/10.1002/rob.22117 by University Di Roma La Sapienza, Wiley Online Library on [08/04/2024]. See the Terms and Conditions (https://onlinelibrary.wiley.com/terms-and-conditions) on Wiley Online Library for rules of use; OA articles are governed by the applicable Creative Commons License

TABLE 3 Generated plan for a mission involving a UAV for a camera inspection and an IMR robot for an NDT inspection

Expected starting time (s)	Executed action	Expected duration (s)
0.00	(uav_takeoff uav uav_wp0)	[90.0]
90.01	(uav_navigate uav uav_wp0 uav_wp1)	[200.0]
290.02	(uav_inspect_blade uav uav_wp1)	[510.0]
800.03	(uav_deploy_imr uav imr uav_wp1 imr_wp0)	[510.0]
1310.04	(imr_navigate imr imr_wp0 imr_wp1)	[300.0]
1310.04	(uav_navigate uav uav_wp1 uav_wp0)	[200.0]
1510.05	(uav_land uav uav_wp0 uav_wp0)	[90.0]
1600.06	(uav_refuel_home uav uav_wp0)	[160.0]
1610.05	(imr_ndt_inspect imr imr_wp1)	[300.0]
1760.07	(uav_takeoff uav uav_wp0)	[139.5]
1910.06	(imr_navigate imr imr_wp1 imr_wp0)	[300.0]
1935.99	(uav_navigate uav uav_wp0 uav_wp1)	[274.0]
2210.07	(uav_retrieve_irr uav imr uav_wp1 imr_wp0)	[510.0]
2720.08	(uav_navigate uav uav_wp1 uav_wp0)	[200.0]
2920.09	(uav_land uav uav_wp0)	[90.0]

actuator malfunctions resulting in a failure in the execution of the actions. For example, a failure action of retrieving a blade IMR robot `uav_retrieve_irr(?uav,?imr,?uav_wp,?imr_wp)` can come from a failed engagement between the OLAM attached to the blade IMR robot and the LHM attached to the UAV. Through access to sensors and actuators via MAVROS, the GMP dynamically monitors any discrepancy between the actual sensors' output and the expected one. For any failed action, a correction to the action-related discrepancies is made by correcting the corresponding predicate values associated with the actions stored in the KB module. The GMP will then trigger replanning to redeem the action failures that have happened.

In PDDL, these sensor outputs are represented as Boolean predicates. These predicates correspond to either a sensor functionality or a binary detection. For example, a predicate `attached_to(?imr,?uav)` represents a sensor detection on the hook of the LHM module that indicates whether a blade IMR robot is hooked into a UAV or not. A predicate `has_retrieval_system(?uav)` represents a complete LHM module attached to a UAV and specifies whether the LHM is fully functional or not. Some of these sensor outputs correspond to a goal of a mission, and they are: `turbine_inspected_at(?wp)`, `turbine_nd_tested_at(?wp)`, `turbine_repaired_at(?wp)`. These goals are effects of the actions `uav_inspect_blade(?uav,?wp)`, `imr_ndt_inspect(?imr,?wp)`, and `imr_repair_wt(?imr,?wp)`. As an example, the expected sensor output of the action `uav_inspect_blade(?uav,?wp)` is that a wind blade is fully scanned, which translates into the goal predicate `turbine_inspected_at(?wp)` being true.

We use a procedural approach to action refinement and execution monitoring. A function that refines an action operator, for example, `uav_inspect_wt(?uav,?wp)`, into low-level commands resides on each vehicle control interface (shown in Figure 15). Each of these functions communicates its completion of the action to the problem generator. A failed output from a function triggers the problem generator to remove the corresponding predicates and request a replanning to ROSPlan, while a successful output triggers the problem generator to add the effect predicates of the action to the KB. Figure 16 shows a plan of the IMR robot retrieval mission with its crucial state transition during the execution of an action. Each action block implementation resides in the UAV/IMR robot control interface module, while the state transition process (i.e., changing the effect of an action) is implemented in the problem generator module. One should note that the precondition states and effect states of each action are not limited to what is pictured in Figure 16. Other states such as robot's battery/fuel level, the availability of the sensor/actuator, and whether the involving robots are busy are also considered as preconditions of each action to ensure robustness in the generated plans.[4] Replanning is also implicitly tailored to the action that has failed. For example, in the case of insufficient fuel during a mission, the current mission will be aborted, and a replan must be requested that prioritizes all robots returning to shore/ground.

6 | EXPERIMENTS

To validate the developed prototype systems, four experiments have been conducted, including field tests of UAV navigation, LHM verification experiments, a field tests of the RDI and field tests of

[4]A complete precondition for each action can be found in our planning domain.

15564967, 2023, 1, Downloaded from https://onlinelibrary.wiley.com/doi/10.1002/rob.22117 by University Di Roma La Sapienza, Wiley Online Library on [08/04/2024]. See the Terms and Conditions (https://onlinelibrary.wiley.com/terms-and-conditions) on Wiley Online Library for rules of use; OA articles are governed by the applicable Creative Commons License

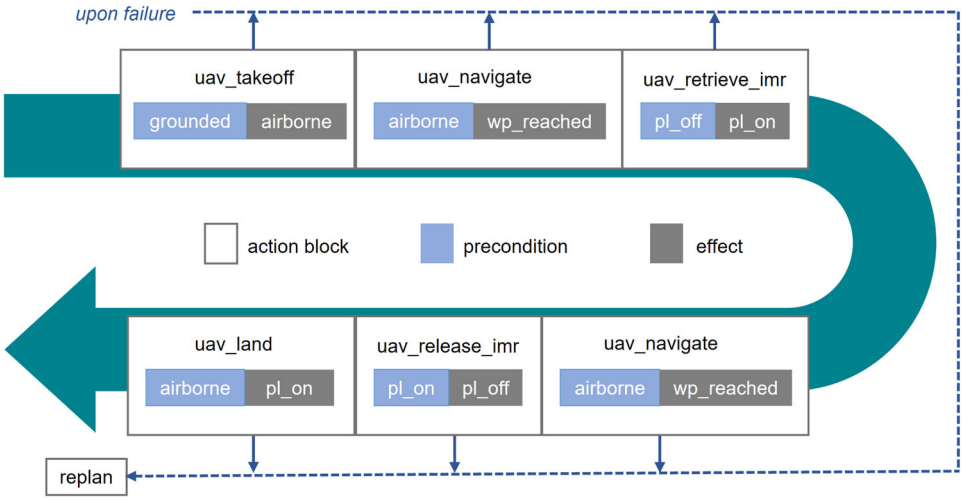

FIGURE 16 A generated plan for an IMR robot retrieval mission focusing on the internal state transition of each action. Crucial states, both precondition and effect, are presented in the action block. If the effect of an action is not met after the execution, a replan will be requested by the problem generator module.

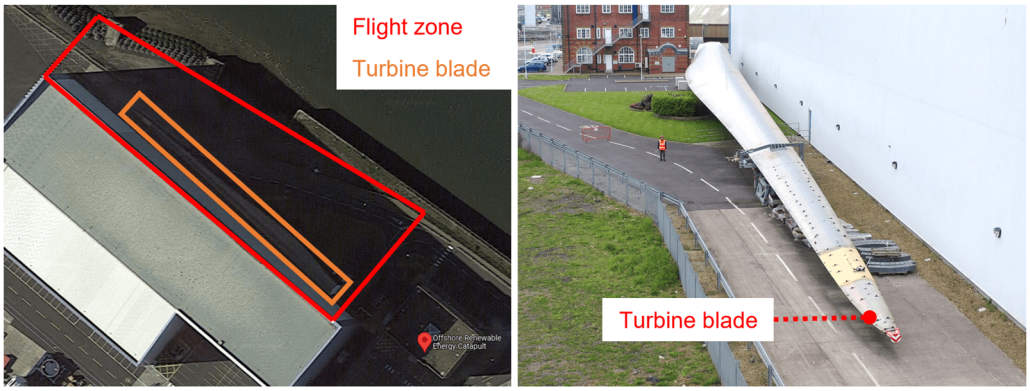

FIGURE 17 Test site with a retired wind turbine blade

the retrieval system. Two test sites have been used to facilitate these experiments. The LHM verification test was conducted in Fenswood Farm which provides a large open space flight area, and the remaining experiments were carried out at a test site with a retired wind turbine blade, as shown in Figure 17. The wind turbine blade was horizontally supported on several pedestals that raised the blade approximately 1–2 m from the ground.

Videos of the trials are available at https://youtube.com/playlist?list=PL5mJodtGpCe3bltNFwgP0_OCRPRt6-dUS.

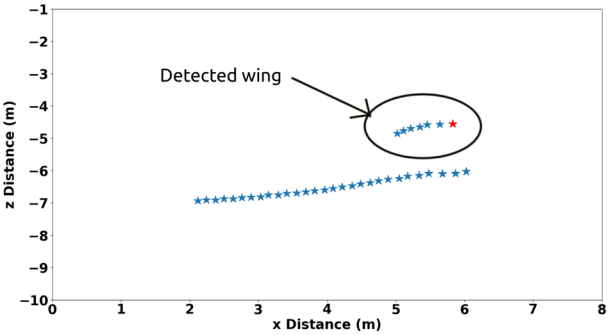

FIGURE 18 LiDAR scan from WP1 as defined in Figure 13 (preset at 6 m in front and 5 above the wing)

6.1 | Field test of UAV navigation

A novel navigation system, as outlined in Section 4, has been developed for the UAV to accurately place the IMR robot at the highest point on the turbine blade at a given distance from the wind turbine's hub. To verify the performance, a retired turbine blade placed horizontally near ground level (see Figure 17) was used. In these experiments the procedures detailed in Figure 13 in Section 4 have been followed. To investigate repeatability as well as accuracy, the test was repeated four times. Figures 18 and 19 illustrate the processed LiDAR data of two of the scans taken at WP1 (preset at

15564967, 2023, 1, Downloaded from https://onlinelibrary.wiley.com/doi/10.1002/rob.22117 by University Di Roma La Sapienza, Wiley Online Library on [08/04/2024]. See the Terms and Conditions (https://onlinelibrary.wiley.com/terms-and-conditions) on Wiley Online Library for rules of use; OA articles are governed by the applicable Creative Commons License

6 m in front and 5 m above the wing) and WP2 (preset at 3.5 m in front and 5 m above the wing). In these figures, the range vectors have been broken down into *x* distance in front and *z* distance below the UAV. The red points in these figures illustrate the target location (highest point on the wing) to deploy the IMR. The turbine blade in these figures has been identified by detecting the jumps in the LiDAR range data.

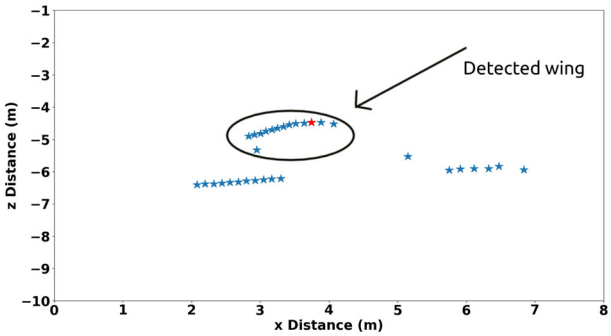

FIGURE 19 LiDAR scan from WP2 as defined in Figure 13 (preset at 3.5 m in front and 5 above the wing)

TABLE 4 LiDAR blade detection results

Test	WP1 (*x*,*z*)	LiDAR WP1 (*x*,*z*)	WP2 (*x*,*z*)	LiDAR WP2 (*x*,*z*)
#1	(6, 5)	(6.3, 4.9)	(3, 5)	(3.2, 5.1)
#2	(6, 5)	(6.4, 4.7)	(3, 5)	(3.8, 4.5)
#3	(6, 6)	(6.5, 6.0)	(3, 5)	(2.8, 6.3)
#4	(10, 5)	(9.4, 5.7)	(5, 5)	(5.2, 5.5)

Note: Distances are given in meters.

TABLE 5 LiDAR blade detection accuracy results

Direction	WP1	WP2	Overall
x	0.45	0.85	0.65
z	0.28	0.6	0.44

Note: Data are all in meters.

Table 4 shows the results from the four localization trials. In this table, WP1 and WP2 are the predefined waypoints with reference to the landing location. The UAV has used its internal system navigation (Extended Kalman filter using gyroscopes, accelerometer, compass, GNSS, and barometric pressure) to get to these points where LiDAR scans have been conducted for localization which have then been compared with the UAV knowledge. In the table below, LiDAR WP1 and LiDAR WP2 are the detected distances to the landing location. As the results suggest, the process has been repeatable.

Table 5 contains the accuracy in LiDAR measurements compared to the UAV's location knowledge. As it can be deduced, there has been a higher accuracy in the *z* direction compared to *x* direction. This could be due to the fact that UAV localization is more accurate in the *z*-direction (as a barometric pressure is also used). However, to gain a better understanding of the performance and accuracy, an external monitoring system is needed in the future.

6.2 | Field test of the robot deployment interface

An RDI prototype was built and tested in a field experiment using Goliath as the UAV platform. The payload for deployment is a dummy OLAM installed on a BladeBug MK II mockup, as shown in Figure 20. The mockup has a representative size and weighs 2.3 kg. The whole payload weighs approximately 3.5 kg.

Since Goliath had not been integrated with the navigation system, it was controlled manually by a human pilot using a remote controller. Due to difficulties in manually determining the correct landing spot, Goliath was not landed on the blade during deployment. Instead, it was flying in hover closely above the blade surface. The experiment was repeated twice, and in both attempts, the payload was successfully deployed. Figure 21 shows the sequence of actions recorded during one of the attempts.

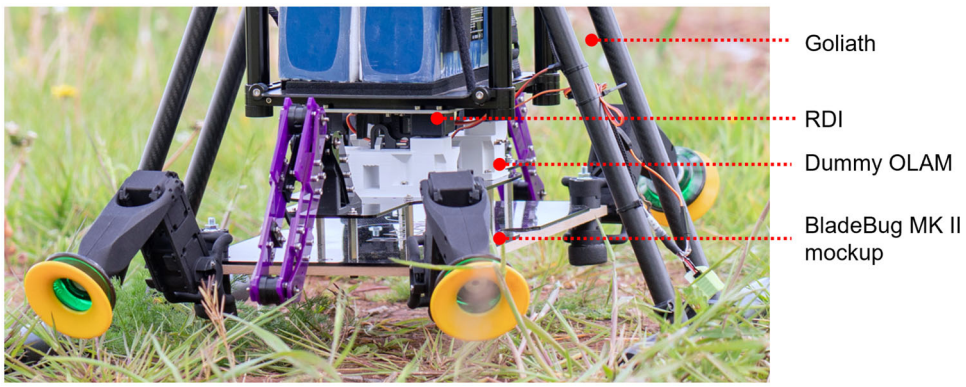

FIGURE 20 RDI installed in Goliath with a dummy OLAM prototype attached

15564967, 2023, 1, Downloaded from https://onlinelibrary.wiley.com/doi/10.1002/rob.22117 by University Di Roma La Sapienza, Wiley Online Library on [08/04/2024]. See the Terms and Conditions (https://onlinelibrary.wiley.com/terms-and-conditions) on Wiley Online Library for rules of use; OA articles are governed by the applicable Creative Commons License

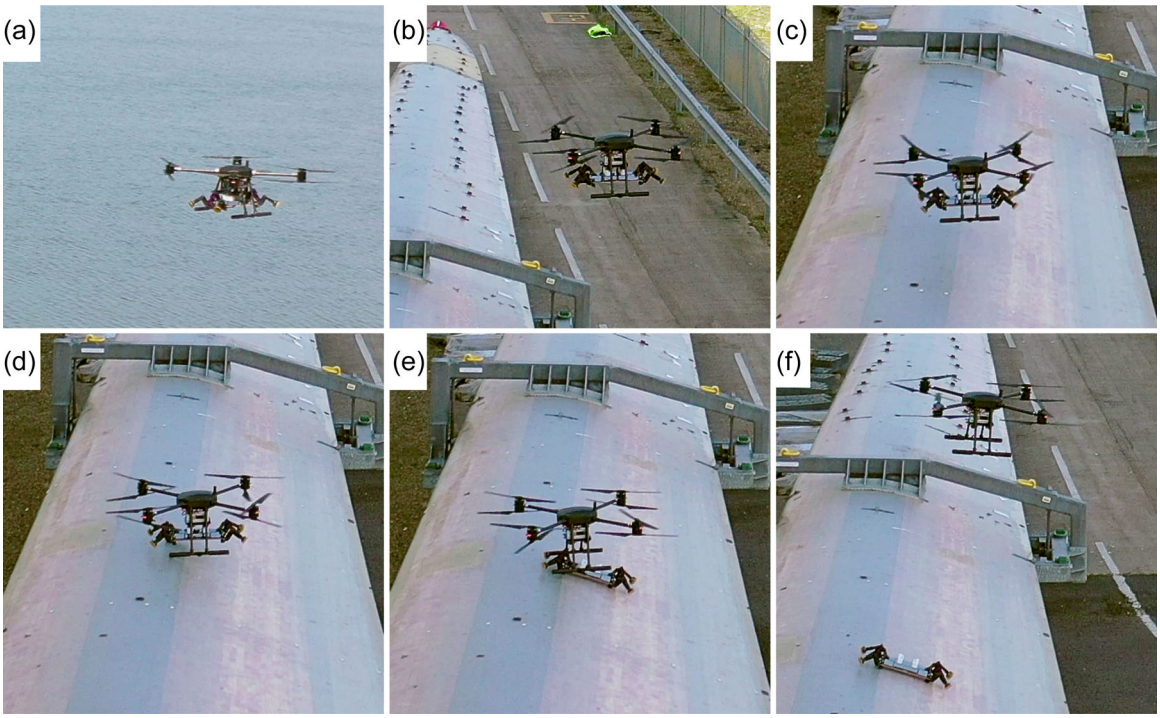

FIGURE 21 Sequence of actions of deploying the mockup IMR robot using Goliath and the RDI prototype: (a,b) approaching the wind turbine blade from afar, (c,d) hovering above the landing spot, (e) releasing the robot, and (f) returning to land.

FIGURE 22 LHM attached to Goliath

6.3 | LHM verification experiment

As discussed in Section 3.4, the LHM is designed with a swing reduction function to reduce the pendulum motion of the hook during the engagement stage. This experiment aims to evaluate both passive and active swing reduction modes implemented on the LHM prototype (see Figure 22) when there is no payload attached to the hook to mimic the engagement scenario. In addition, the experiment was extended to evaluate the ability to stabilize a heavy payload using both passive and active swing reduction.

Four sets of tests were conducted, as detailed in Table 6, to validate the performance of the prototype LHM. Goliath was used as the UAV platform and the payload used in the extension experiment weighed approximately 3.1 kg, attached to the hook by a 300 mm Polypropylene rope. Goliath was piloted manually to take off and then Mission Planner took control and flew Goliath in auto mode to traverse in a straight line between two waypoints at a speed of 6 m/s as shown in Figure 23. The waypoints were set to be 11 m apart for the first two sets of tests where no payload was attached to the hook. The distance was made short to encourage Goliath to perform more aggressive maneuvers with increased acceleration and deceleration, hence, to stress test the LHM. In the extension experiment, where the payload was attached to the hook, this distance was increased to 23 m to reduce acceleration, avoiding excessive pendulum motion that may turn the system into an unstable mode. The first two sets of tests were repeated three times and the next two sets were repeated six times since more variation in the swing motion was observed. A round trip between the waypoints was considered as one repetition. After Test #1 and Test #3, the UAV was commanded to hover and the active swing reduction function was remotely switched on before the experiment continued. The UAV was brought to landing before the extension experiment and the batteries were recharged to full. The average wind speed during Test #1 and #2 was approximately 6.1 with 9.2 m/s gust and during Test #3 and #4 was 7.2 with 8.6 m/s gust. The joint angles of the 2-DoF hinge on the LHM and power consumption of the hinge were recorded during the experiment.

15564967, 2023, 1, Downloaded from https://onlinelibrary.wiley.com/doi/10.1002/rob.22117 by University Di Roma La Sapienza, Wiley Online Library on [08/04/2024]. See the Terms and Conditions (https://onlinelibrary.wiley.com/terms-and-conditions) on Wiley Online Library for rules of use; OA articles are governed by the applicable Creative Commons License

TABLE 6 Details of the LHM verification test

Test	Wind speed (m/s)	Gust speed (m/s)	Waypoint distance (m)	Velocity (m/s)	Mode	Payload	Repetition
#1	6.1	9.2	11	6	Passive	None	3
#2	6.1	9.2	11	6	Active	None	3
#3	7.2	8.6	23	6	Passive	3.1 kg	6
#4	7.2	8.6	23	6	Active	3.1 kg	6

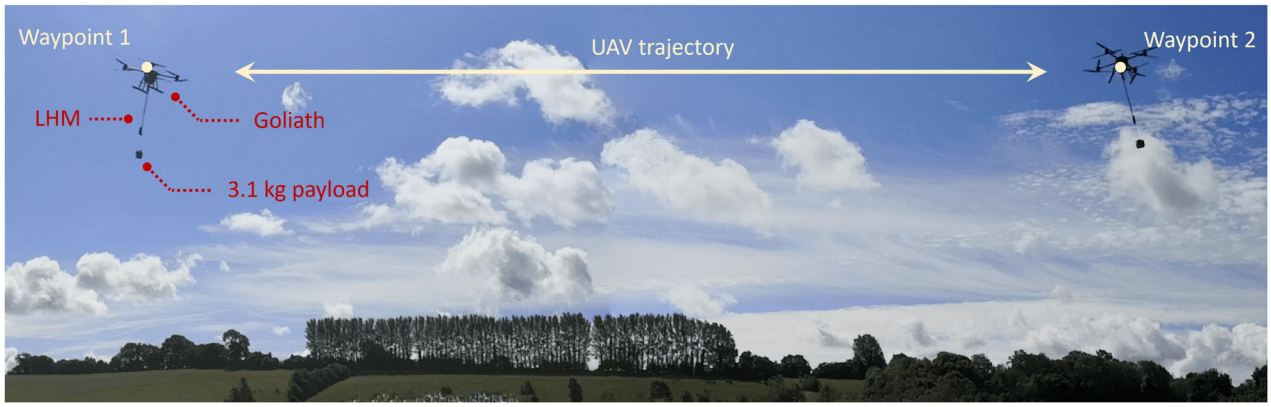

FIGURE 23 LHM verification experimental setup

TABLE 7 Mean velocity and acceleration achieved by Goliath

Test	Mean velocity (m/s)	Mean acceleration (m/s^2)
#1	2.9	0.53
#2	2.9	0.53
#3	4.4	0.38
#4	4.4	0.38

6.3.1 | Results

The flight log produced by Goliath's flight computer was retrieved and analysed. As can be seen from Table 7, the mean velocities achieved by Goliath during the test were lower than the target velocity. This is because the UAV had been tuned for a smooth flight with stability prioritized over agility, and therefore, not able to reach the target speed within a short distance.

The longitudinal and lateral displacement of the hook was calculated using forward kinematics and the result is visualized in Figure 24. Table 8 shows the mean and standard deviation of the displacement. In passive swing reduction mode, with a 3.1 kg payload, the pendulum motion was over two times greater in magnitude than it was without a payload. The use of active mode reduces the mean displacement of the hook by approximately 30% (longitudinal) to 34% (lateral) and standard deviation by 23% (longitudinal) to 34% (lateral). Similar reductions can also be observed for the scenario without the payload, although the improvement in lateral displacement and variation is less significant. This is possibly due to the presence of strong lateral gust wind during Test #2, which could also explain that the maximum lateral displacement is slightly greater in Test #2 compared with Test #1 (as 159.9 vs. 155.9 mm).

The power consumption of the hinge was found reasonably low. In active swing reduction mode, with and without payload, the two servos drew 28.22 and 7.27 mA, respectively, at 12 V on average.

6.4 | Field test of the retrieval system

An integrated retrieval system involving Goliath, the LHM prototype (see Figure 22), the OLAM prototype (see Figure 25), and the GMP has been built, and a field trial for the retrieval system was conducted. Since the OLAM prototype was manufactured with rapid prototyping methods, including 3D printing and laser cutting Perspex, the strength of its structure is lacking and the BladeBug mockup was not used. In addition, the arms of the OLAM are fixed in the raised position instead of being servo actuated.

As shown in Figure 26, the OLAM prototype was placed on the wind turbine blade and the LHM was attached to Goliath.

15564967, 2023, 1, Downloaded from https://onlinelibrary.wiley.com/doi/10.1002/rob.22117 by University Di Roma La Sapienza, Wiley Online Library on [08/04/2024]. See the Terms and Conditions (https://onlinelibrary.wiley.com/terms-and-conditions) on Wiley Online Library for rules of use; OA articles are governed by the applicable Creative Commons License

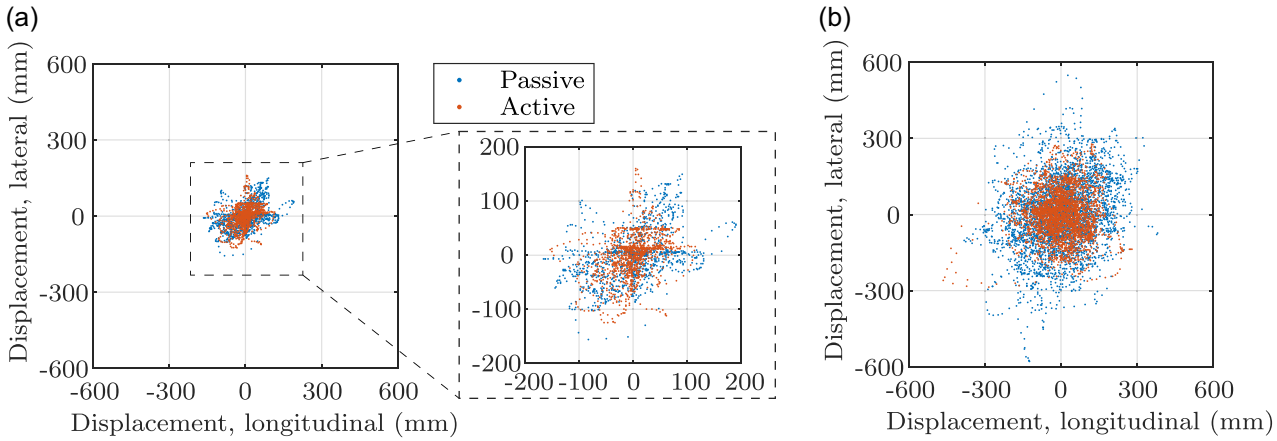

FIGURE 24 Variation of hook positions in lateral and longitudinal directions, (a) without payload and (b) with a 3.1 kg payload.

TABLE 8 Mean and standard deviation of the displacement of the hook in longitudinal and lateral directions

Test	Mean displacement		SD	
	Longitudinal	Lateral	Longitudinal	Lateral
#1	47.40	35.83	38.02	33.30
#2	29.05	31.37	26.11	27.86
#3	93.23	107.03	70.67	87.19
#4	65.01	70.89	54.12	57.25

FIGURE 25 OLAM prototype

Both Goliath and the OLAM prototype were fully automated and controlled by the GMP described in Section 5. A safety pilot was present to take over in the event of potential hazards. The average wind speed during the experiment was 5.0 with 5.8 m/s gust.

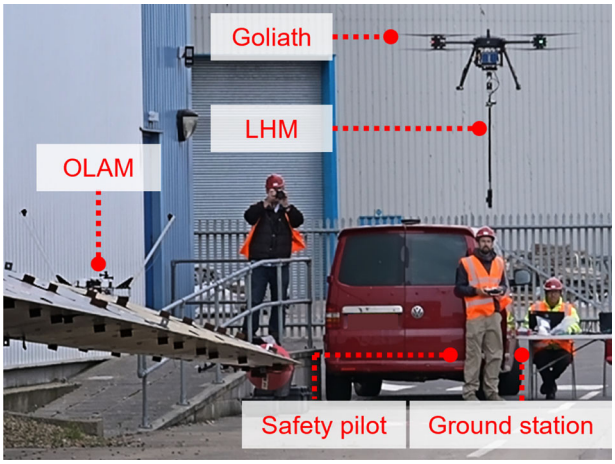

FIGURE 26 Retrieval system trial setup

A full plan for the whole mission was automatically generated by the GMP based on real-time data supplied by Goliath and the OLAM. These data include OLAM GPS position, LHM status, battery level, Goliath rotors' states, and so on. The trajectory of the UAV and its corresponding action during the test is illustrated in Figure 27. Figure 28 shows the sequence of actions during the mission. Goliath first took off from the ground (a, b) and then approached the OLAM based on the GPS location (c). Next, Goliath aligned the LHM with the pickup line so that the hook was at the correct attitude and lined up with the center of the pickup line (d). Goliath then flew in a straight line until engagement was detected (e) when Goliath started to gain attitude (f) and travel to a predefined location to release the OLAM (g, h). After the OLAM was landed safely, the LHM was commanded to move into the landing position (i–k) and finally, Goliath landed (l). The entire process was fully automated without human intervention.

15564967, 2023, 1, Downloaded from https://onlinelibrary.wiley.com/doi/10.1002/rob.22117 by University Di Roma La Sapienza, Wiley Online Library on [08/04/2024]. See the Terms and Conditions (https://onlinelibrary.wiley.com/terms-and-conditions) on Wiley Online Library for rules of use; OA articles are governed by the applicable Creative Commons License

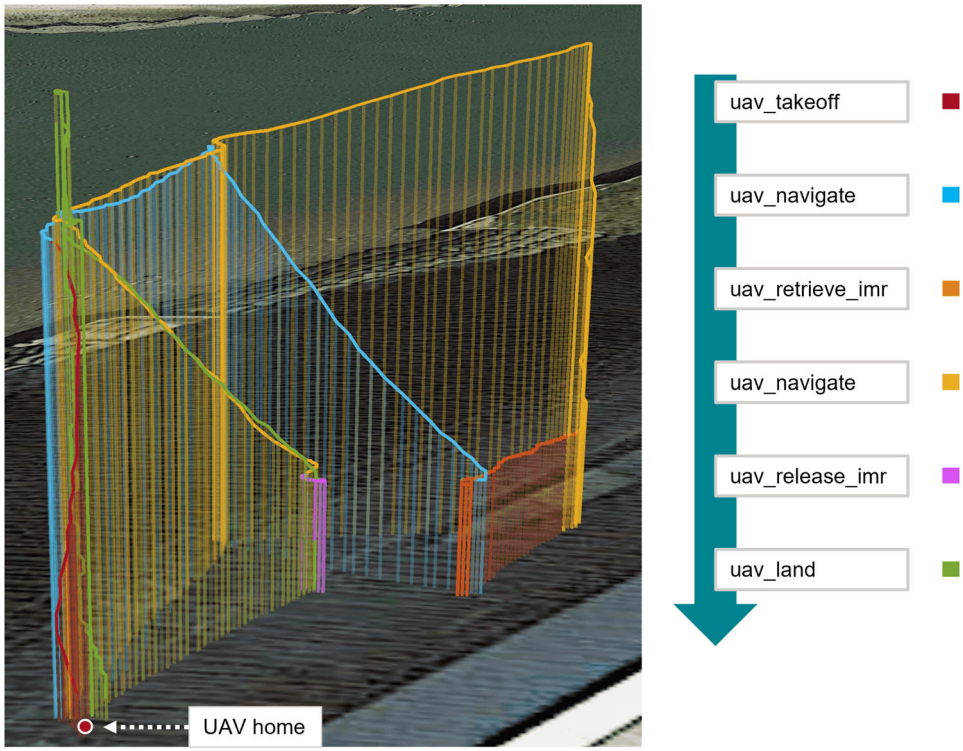

FIGURE 27 UAV trajectory and corresponding actions as planned by the global mission planner (GMP)

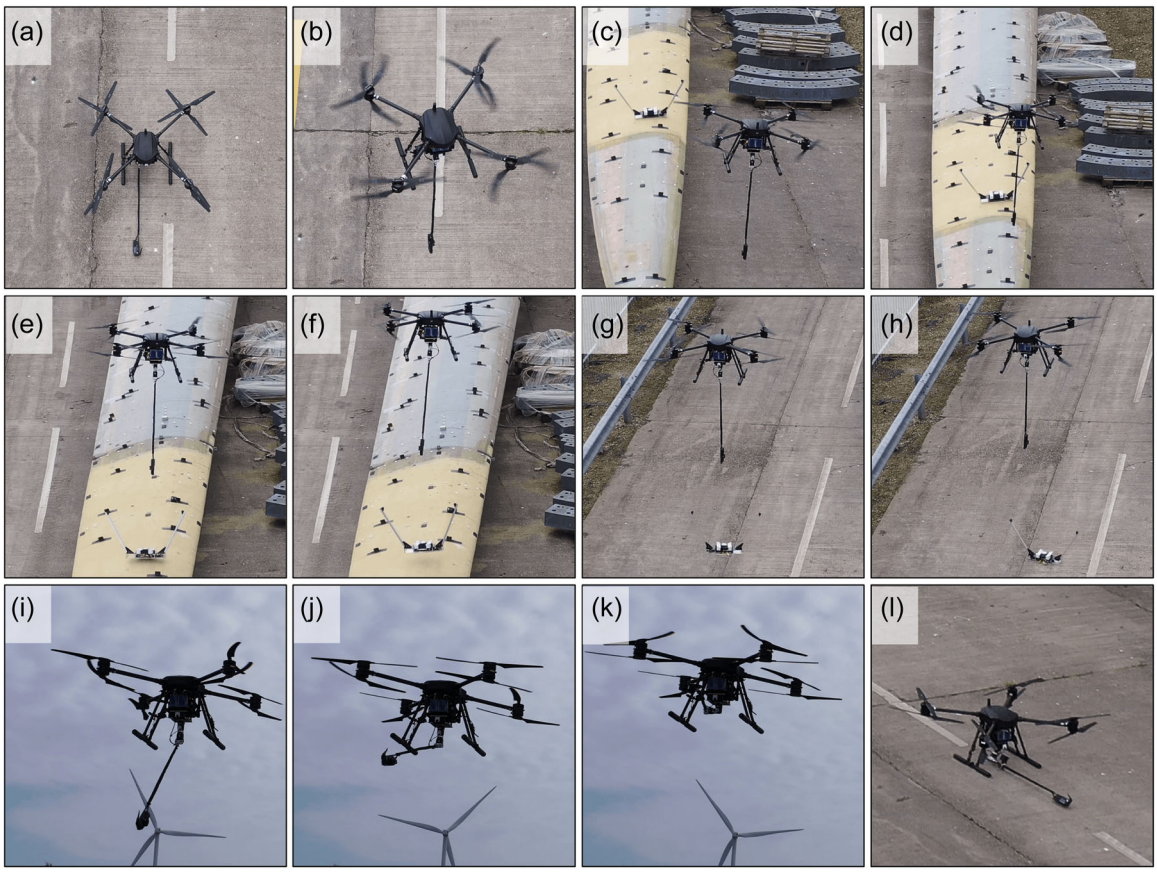

FIGURE 28 Action sequence of retrieving the OLAM using Goliath and the LHM: (a, b) taking off, (c, d) approaching and lining up with the OLAM, (e, f) engaging and lifting the OLAM from the blade surface, (g, h) releasing the OLAM, (i–k) folding the LHM and (l) landed.

15564967, 2023, 1, Downloaded from https://onlinelibrary.wiley.com/doi/10.1002/rob.22117 by University Di Roma La Sapienza, Wiley Online Library on [08/04/2024]. See the Terms and Conditions (https://onlinelibrary.wiley.com/terms-and-conditions) on Wiley Online Library for rules of use; OA articles are governed by the applicable Creative Commons License

7 | CONCLUSIONS

This study looks into the benefit of combining robot retrieval and deployment with autonomous UAVs to perform IMR tasks on offshore wind turbines. These are sophisticated tasks that require particular retrieval and deployment systems, smart navigation around wind blades, and accurate autonomy that manages and guides the whole task from start to end.

A novel deployment and retrieval system is introduced to overcome the challenges in safely deploying and recovering an IMR robot from a wind turbine. A UAV navigation system has been developed to safely and autonomously land the UAV on a wind turbine blade. Mechatronic systems for unmanned deploying and retrieving IMR robots from wind turbine blades have been designed and developed. A complex PDDL model and a powerful autonomy architecture have been developed to underpin the execution of these IMR tasks. A strategy was devised to correct the domain and problem specification by monitoring the discrepancies between the expected and the actual states of the actions over time. A correction to the knowledge base is made after every action representing a current corrected state, a replanning is requested, and an appropriate plan is automatically generated.

Individual modules of the proposed system have been validated in field trials. The results show the UAV was able to safely navigate around the wind turbine blade and successfully located an appropriate landing spot for deploying the IMR robot. The manual IMR robot deployment trial suggested the effectiveness of the developed mechatronic prototype. The proposed retrieval system has been fully integrated with the UAV and the GMP, which was validated in representative scenarios with a mock-up IMR robot and a wind turbine blade. Our experiments show that the proposed approach is effective in retrieving an IMR robot from a wind turbine blade safely and robustly without the need for human interventions.

In future work, the deployment system will be fully integrated and tested to complete the proposed autonomous system. The effect of high-speed wind gusts (over 10 m/s) on the system, which is typical near wind turbine blades must also be further investigated. The prototypes were constructed using 3D printed components, which limits the strength and hence payload capacity of the system. Further work is needed in completing the system using more appropriate manufacturing methods and mechanical materials to test a full-size and functional IMR robot.

ACKNOWLEDGMENT

This study has received funding from UKRI through the Innovate UK Grant Agreement No. 104821 and EPSRC Grant EP/R026084/1.

DATA AVAILABILITY STATEMENT

The data that support the findings of this study are available from the corresponding author upon reasonable request.

ORCID

Zhengyi Jiang http://orcid.org/0000-0001-6528-4209
Simon Watson http://orcid.org/0000-0001-9783-0147

REFERENCES

Appius, A. X., Bauer, E., Blochlinger, M., Kalra, A., Oberson, R. & Raayatsanati, A. et al. (2022) Raptor: rapid aerial pickup and transport of objects by robots. ArXiv, abs/2203.03018. https://doi.org/10.48550/arXiv.2203.03018

Bergström, L., Kautsky, L., Malm, T., Rosenberg, R., Wahlberg, M., Capetillo, N. Å. & Wilhelmsson, D. (2014) Effects of offshore wind farms on marine wildlife—A generalized impact assessment. *Environmental Research Letters*, *9*(3), 034012.

Bernardini, S., Jovan, F., Jiang, Z., Watson, S., Weightman, A., Moradi, P., Richardson, T., Sadeghian, R. & Sareh, S. (2020) A multi-robot platform for the autonomous operation and maintenance of offshore wind farms. In: *AAMAS'20*, pp. 1696–1700.

Carreno, Y., Ng, J. H. A., Petillot, Y. & Petrick, R. (2022) Planning, execution, and adaptation for multi-robot systems using probabilistic and temporal planning. In: *Proceedings of the 21st International Conference on Autonomous Agents and Multiagent Systems*, AAMAS'22. Richland, SC: International Foundation for Autonomous Agents and Multiagent Systems, pp. 217–225.

Carreno, Y., Petrick, R. P. A. & Petillot, Y. (2019) Multi-agent strategy for marine applications via temporal planning. In: 2019 IEEE Second International Conference on Artificial Intelligence and Knowledge Engineering (AIKE), pp. 243–250. https://doi.org/10.1109/AIKE.2019.00049

Cashmore, M., Fox, M., Long, D., Magazzeni, D., Ridder, B., Carrera, A., Palomeras, N., Hurtos, N. & Carreras, M. (2015) ROSPlan: Planning in the robot operating system, *Proceedings of the International Conference on Automated Planning and Scheduling, Jerusalem, Israel*, Vol 25, pp. 333–341.

Coles, A. J., Coles, A. I., Fox, M. & Long, D. (2010) Forward-chaining partial-order planning. In: Proceedings of the 20th International Conference on Automated Planning Scheduling. CAN.

Fernandez-Gonzalez, E., Karpas, E. & Williams, B. C. (2017) Mixed discrete-continuous planning with convex optimization. In: AAAI-2017, pp. 4574–4580.

Fiaz, U. A., Abdelkader, M. & Shamma, J. S. (2018) An intelligent gripper design for autonomous aerial transport with passive magnetic grasping and dual-impulsive release. In: 2018 IEEE/ASME International Conference on Advanced Intelligent Mechatronics (AIM), pp. 1027–1032. https://doi.org/10.1109/aim.2018.8452383

Fiaz, U. A., Toumi, N. & Shamma, J. S. (2017) Passive aerial grasping of ferrous objects. *IFAC-PapersOnLine*, *50*(1), 10299–10304. https://doi.org/10.1016/j.ifacol.2017.08.1495

Fox, M. & Long, D. (2003) PDDL2.1: an extension to PDDL for expressing temporal planning domains. *Journal of Artificial Intelligence Research*, *20*, 61–124. https://doi.org/10.1613/jair.1129

Heinrich, S., Humbert, A. & Amiel, R. (2018) GreenSpace and reuse scenarios for launcher industry. In: *2018 SpaceOps Conference*. Marseille, France, p. 2600. https://doi.org/10.2514/6.2018-2600

IRENA (2019). Future of wind: deployment, investment, technology, grid integration and socio-economic aspects. International Renewable Energy Agency, Abu Dhabi. Available at: https://www.irena.org/-/media/files/irena/agency/publication/2019/oct/irena_future_of_wind_2019.pdf

Ivanovic, A., Polic, M., Salah, O., Orsag, M. & Bogdan, S. (2018) Compliant net for AUV retrieval using a UAV. *IFAC-PapersOnLine*, *51*(29), 431–437.

Jovan, F. & Bernardini, S. (2021) Multi-robot coordination in operations and maintenance of off shore wind farms with temporal planning. *Proceedings of the International Conference on Automated Planning and Scheduling*, *31*(1). https://icaps21.icaps-conference.org/demos/demos/380.pdf

Kabbabe Poleo, K., Crowther, W. J. & Barnes, M. (2021) Estimating the impact of drone-based inspection on the levelised cost of electricity for offshore wind farms. *Results in Engineering*, *9*, 100201. https://doi.org/10.1016/j.rineng.2021.100201

15564967, 2023, 1, Downloaded from https://onlinelibrary.wiley.com/doi/10.1002/rob.22117 by University Di Roma La Sapienza, Wiley Online Library on [08/04/2024]. See the Terms and Conditions (https://onlinelibrary.wiley.com/terms-and-conditions) on Wiley Online Library for rules of use; OA articles are governed by the applicable Creative Commons License

Kamat, S. U. & Rasane, K. (2018) A survey on autonomous navigation techniques. In: *2018 Second International Conference on Advances in Electronics, Computers and Communications (ICAECC)*. IEEE, pp. 1–6. https://doi.org/10.1109/ICAECC.2018.8479446

Leary, W. M. (2008) Robert Fulton's skyhook and operation coldfeet. Central Intelligence Agency. Available at: https://apps.dtic.mil/sti/citations/ADA528051

Lee, J. & Zhao, F. (2021) Global wind report 2021. Global Wind Energy Council. Available at: https://gwec.net/wp-content/uploads/2021/03/GWEC-Global-Wind-Report-2021.pdf

Lugo, J. J. & Zell, A. (2014) Framework for autonomous on-board navigation with the AR.Drone. *Journal of Intelligent & Robotic Systems*, *73*(1-4), 401–412. https://doi.org/10.1109/ICUAS.2013.6564735

Luo, C., Yang, S. X., Krishnan, M., Paulik, M. & Chen, Y. (2013) A hybrid system for multi-goal navigation and map building of an autonomous vehicle in unknown environments. In: *2013 IEEE International Conference on Robotics and Biomimetics (ROBIO)*. IEEE, pp. 1228–1233. https://doi.org/10.1109/ROBIO.2013.6739632

Nilsson, J. & Bertling, L. (2007) Maintenance management of wind power systems using condition monitoring systems–life cycle cost analysis for two case studies. *IEEE Transactions on Energy Conversion*, *22*(1), 223–229. https://doi.org/10.1109/TEC.2006.889623

Nonnenmacher, D. & Jones, M. (2016) Handling qualities evaluation of an automatic slung load stabilization system for rescue hoist operations. *CEAS Aeronautical Journal*, *7*, 587–606. https://doi.org/10.1007/s13272-016-0211-6

Nordin, M. H., Sharma, S., Khan, A., Gianni, M., Rajendran, S. & Sutton, R. (2022) Collaborative unmanned vehicles for inspection, maintenance, and repairs of offshore wind turbines. *Drones*, *6*(6), 137.

Patruno, C., Nitti, M., Petitti, A., Stella, E. & D'Orazio, T. (2019) A vision-based approach for unmanned aerial vehicle landing. *Journal of Intelligent & Robotic Systems*, *95*(2), 645–664. https://doi.org/10.1007/s10846-018-0933-2

Piacentini, C., Bernardini, S. & Beck, J. C. (2019) Autonomous target search with multiple coordinated uavs. *Journal of Artificial Intelligence Research*, *65*, 519–568. https://doi.org/10.1613/jair.1.11635

Rao, Y., Xiang, B. J., Huang, B. & Mao, S. (2019) Wind turbine blade inspection based on unmanned aerial vehicle (uav) visual systems. In: 2019 IEEE 3rd Conference on Energy Internet and Energy System Integration (EI2), pp. 708–713.

Ren, Z., Verma, A. S., Li, Y., Teuwen, J. J. & Jiang, Z. (2021) Offshore wind turbine operations and maintenance: a state-of-the-art review. *Renewable and Sustainable Energy Reviews*, *144*, 110886. https://doi.org/10.1016/j.rser.2021.110886

Roderick, W. R. T., Cutkosky, M. R. & Lentink, D. (2021) Bird-inspired dynamic grasping and perching in arboreal environments. *Science Robotics*, *6*(61), eabj7562. https://doi.org/10.1126/scirobotics.abj7562

Schäfer, B. E., Picchi, D., Engelhardt, T. & Abel, D. (2016) Multicopter unmanned aerial vehicle for automated inspection of wind turbines. In: *2016 24th Mediterranean Conference on Control and Automation (MED)*. IEEE, pp. 244–249. https://doi.org/10.1109/MED.2016.7536055

Stetco, A., Dinmohammadi, F., Zhao, X., Robu, V., Flynn, D., Barnes, M., Keane, J. & Nenadic, G. (2019) Machine learning methods for wind turbine condition monitoring: a review. *Renewable Energy*, *133*, 620–635. https://doi.org/10.1016/j.renene.2018.10.047

Thomas, J., Polin, J., Sreenath, K. & Kumar, V. (2013) Avian-inspired grasping for quadrotor micro UAVs. Volume 6A. In: *37th Mechanisms and Robotics Conference of International Design Engineering Technical Conferences and Computers and Information in Engineering Conference*. https://doi.org/10.1115/DETC2013-13289

Tscholl, D., Gravert, S.-D., Appius, A. X. & Katzschmann, R. K. (2022) Flying hydraulically amplified electrostatic gripper system for aerial object manipulation. ArXiv, abs/2205.13011. https://doi.org/10.48550/arXiv.2205.13011

Tsiropoulos, I., Nijs, W., Tarvydas, D. & Ruiz, P. (2020) Towards net-zero emissions in the eu energy system by 2050. In: Insights from Scenarios in Line with the 2030 and 2050 Ambitions of the European Green Deal. https://doi.org/10.2760/062347

Venugopalan, T., Taher, T. & Barbastathis, G. (2012) Autonomous landing of an unmanned aerial vehicle on an autonomous marine vehicle. In: *2012 Oceans*. IEEE, pp. 1–9. https://doi.org/10.1109/OCEANS.2012.6404893

Welburn, E., Wright, T., Marsh, C., Lim, S., Gupta, A., Crowther, B. & Watson, S. (2019) A mixed reality approach to robotic inspection of remote environments. In: *Proceedings of the Second UK-RAS Conference*. UK-RAS, pp. 72–74.

Young, L. A. (2007) Enhanced rescue lift capability. In: *63rd Annual Forum of the AHS International*. Virginia Beach, VA.

Zion Market Research. (2019) Wind turbine operations and maintenance market by application (offshore and onshore): global industry perspective, comprehensive analysis, and forecast, 2018–2025. Zion Market Research Reports.

How to cite this article: Jiang, Z., Jovan, F., Moradi, P., Richardson, T., Bernardini, S., Watson, S., et al. (2023) A multirobot system for autonomous deployment and recovery of a blade crawler for operations and maintenance of offshore wind turbine blades. *Journal of Field Robotics*, 40, 73–93. https://doi.org/10.1002/rob.22117

15564967, 2023, 1, Downloaded from https://onlinelibrary.wiley.com/doi/10.1002/rob.22117 by University Di Roma La Sapienza, Wiley Online Library on [08/04/2024]. See the Terms and Conditions (https://onlinelibrary.wiley.com/terms-and-conditions) on Wiley Online Library for rules of use; OA articles are governed by the applicable Creative Commons License